Contrib Mineral Petrol (2017) 172:40
DOI 10.1007/s00410-017-1356-y

ORIGINAL PAPER

Combined iron and magnesium isotope geochemistry of pyroxenite xenoliths from Hannuoba, North China Craton: implications for mantle metasomatism

Xin Miao Zhao[1] · Hui Hui Cao[1] · Xue Mi[1,2] · Noreen J. Evans[3] · Yu Han Qi[4] · Fang Huang[4] · Hong Fu Zhang[1,5]

Received: 8 October 2016 / Accepted: 5 April 2017

Abstract We present high-precision iron and magnesium isotopic data for diverse mantle pyroxenite xenoliths collected from Hannuoba, North China Craton and provide the first combined iron and magnesium isotopic study of such rocks. Compositionally, these xenoliths range from Cr-diopside pyroxenites and Al-augite pyroxenites to garnet-bearing pyroxenites and are taken as physical evidence for different episodes of melt injection. Our results show that both Cr-diopside pyroxenites and Al-augite pyroxenites of cumulate origin display narrow ranges in iron and magnesium isotopic compositions (δ^{57}Fe = −0.01 to 0.09 with an average of 0.03 ± 0.08 (2SD, n = 6); δ^{26}Mg = − 0.28 to −0.25 with an average of −0.26 ± 0.03 (2SD, n = 3), respectively). These values are identical to those in the normal upper mantle and show equilibrium inter-mineral iron and magnesium isotope fractionation between coexisting mantle minerals. In contrast, the garnet-bearing pyroxenites, which are products of reactions between peridotites and silicate melts from an ancient subducted oceanic slab, exhibit larger iron isotopic variations, with δ^{57}Fe ranging from 0.12 to 0.30. The δ^{57}Fe values of minerals in these garnet-bearing pyroxenites also vary widely (−0.25 to 0.08 in olivines, −0.04 to 0.25 in orthopyroxenes, −0.07 to 0.31 in clinopyroxenes, 0.07 to 0.48 in spinels and 0.31–0.42 in garnets). In addition, the garnet-bearing pyroxenite shows light δ^{26}Mg (−0.43) relative to the mantle. The δ^{26}Mg of minerals in the garnet-bearing pyroxenite range from −0.35 for olivine and orthopyroxene, to −0.34 for clinopyroxene, 0.04 for spinel and −0.68 for garnet. These measured values stand in marked contrast to calculated equilibrium iron and magnesium isotope fractionation between coexisting mantle minerals at mantle temperatures derived from theory, indicating disequilibrium isotope fractionation. Notably, one phlogopite clinopyroxenite with an apparent later metasomatic overprint has the heaviest δ^{57}Fe (as high as 1.00) but the lightest δ^{26}Mg (as low as −1.50) values of all investigated samples. Overall, there appears to be a negative co-variation between δ^{57}Fe and δ^{26}Mg in the Hannuoba garnet-bearing pyroxenite and in the phlogopite clinopyroxenite xenoliths and minerals therein. These features may reflect kinetic isotopic fractionation due to iron and magnesium inter-diffusion during melt–rock interaction. Such processes play an important role in producing inter-mineral iron and magnesium isotopic disequilibrium and local iron and magnesium isotopic heterogeneity in the subcontinental mantle.

Keywords Iron and magnesium isotopes · Pyroxenite xenoliths · Melt−rock interaction · Lithospheric mantle · North China Craton

Communicated by Franck Poitrasson.

Electronic supplementary material The online version of this article (doi:10.1007/s00410-017-1356-y) contains supplementary material, which is available to authorized users.

✉ Xin Miao Zhao
xinmiao312@mail.iggcas.ac.cn

[1] State Key Laboratory of Lithospheric Evolution, Institute of Geology and Geophysics, Chinese Academy of Sciences, P.O. Box 9825, Beijing 100029, China

[2] University of Chinese Academy of Sciences, Beijing, China

[3] John de Laeter Center, TIGeR, Applied Geology, Curtin University, Perth, WA 6945, Australia

[4] CAS Key Laboratory of Crust-Mantle Materials and Environments, School of Earth and Space Sciences, University of Science and Technology of China, Hefei 230026, China

[5] State Key Laboratory of Continental Dynamics, Department of Geology, Northwest University, Xi'an 710069, China

Published online: 23 May 2017

Introduction

Iron (Fe) and magnesium (Mg) are two of the major constituent chemical elements of common upper mantle minerals and, hence, the Fe and Mg isotope systematics of ultramafic rocks have received wide attention. Previous studies demonstrated that detectable Fe isotope fractionation could occur (up to 1.6‰) in mantle rocks and their minerals (Zhu et al. 2002; Beard and Johnson 2004; Williams et al. 2004, 2005, 2009, 2012; Schoenberg and Blanckenburg 2006; Weyer and Ionov 2007; Zhao et al. 2010, 2012, 2015; Huang et al. 2011; Poitrasson et al. 2013; Macris et al. 2015; An et al. 2017). This isotopic fractionation could have been controlled by mineral structures (Macris et al. 2015; Roskosz et al. 2015), changes in the oxidation state of Fe (Williams et al. 2004, 2005; Dauphas et al. 2009, 2014; Sossi et al. 2012), melt extraction (Williams et al. 2004, 2005; Weyer and Ionov 2007; Teng et al. 2008; Schuessler et al. 2009; Hibbert et al. 2012), the effect of metasomatism (Beard and Johnson 2004; Williams et al. 2005; Weyer and Ionov 2007; Dauphas et al. 2009; Zhao et al. 2010, 2012, 2015; Poitrasson et al. 2013) and/or kinetic isotopic fractionation caused by diffusion (Teng et al. 2011; Weyer and Ionov 2007; Huang et al. 2011; Weyer and Seitz 2012; Zhao et al. 2012, 2015, 2017; Poitrasson et al. 2013). By contrast, analysis of most oceanic basalts and mantle peridotites has shown that the terrestrial mantle has a homogeneous Mg isotopic composition (average $\delta^{26}Mg = -0.25 \pm 0.07$, 2SD) (Teng et al. 2007, 2010, 2017; Handler et al. 2009; Yang et al. 2009; Bourdon et al. 2010; Dauphas et al. 2010; Bizzarro et al. 2011; Huang et al. 2011; Pogge von Strandmann et al. 2011; Liu et al. 2011; Xiao et al. 2013; Lai et al. 2015) and that the fractionation of Mg isotopes during partial melting and magma-differentiation processes is limited in the mantle (<0.07‰ for $\delta^{26}Mg$, Teng et al. 2007, 2010, 2017). However, recent studies have shown that chemical diffusion generates Fe and Mg isotope fractionation in komatiite, zoned olivine and strongly metasomatized mantle xenoliths that exceeds potential equilibrium isotope fractionation by an order of magnitude (Dauphas et al. 2010; Teng et al. 2011; Weyer and Seitz 2012; Sio et al. 2013; Huang et al. 2011; Zhao et al. 2012, 2015; Hu et al. 2016). Therefore, combined analyses of Fe and Mg isotopic compositions from the same sample could provide new insights into mantle processes.

Pyroxenites are an important mantle lithology and are commonly considered important for basalt generation and mantle refertilization (e.g., Bodinier et al. 1990; Hirschmann and Stolper 1996; Sobolev et al. 2005; Beyer et al. 2006; Pilet et al. 2008; Zhang et al. 2009a; LeRoux et al. 2007, 2009; O'Reilly and Griffin 2012). They are commonly believed to have been formed through peridotite–melt interaction in the lithospheric mantle, or to represent remnants of subducted oceanic crust or the product of mafic magma underplating, e.g., cumulative origin in the crust-mantle transitional zone (Dawson et al. 2001, 2007; Xu 2002; Pearson et al. 2004; Liu et al. 2005; Ackerman et al. 2009; Dantas et al. 2009; Zhang et al. 2012; Ying et al. 2013). Therefore, pyroxenite xenoliths entrained in mafic magmas are ideal samples to study in order to elucidate melt migration, infiltration, or circulation in the subcontinental lithosphere. Recently, Williams and Bizimis (2014) found that Fe in garnet pyroxenites from Hawaii was (on average) isotopically heavy ($\delta^{57}Fe = 0.10$–0.27) compared to depleted peridotites ($\delta^{57}Fe = -0.34$ to 0.14). They attributed the origin of relatively heavy Fe isotope values in Hawaiian pyroxenites versus peridotites to fractional crystallization and cumulate forming processes near the base of the oceanic lithosphere. Hu et al. (2016) carried out the first study on Mg isotopic systematics of pyroxenite xenoliths from the North China Craton (NCC). They found large Mg isotopic variations on both the bulk rock and mineral scales in pyroxenite xenoliths and interpreted this to reflect Mg isotope fractionation during mantle metasomatism.

While Fe and Mg isotopic characterization of pyroxenites can enhance our understanding of mantle processes, a systematic, coupled Fe and Mg isotopic study of pyroxenite xenoliths and their constituent minerals has not previously been done. The impact of Fe and Mg isotopic variations in pyroxenite xenoliths on isotopic heterogeneity in the mantle and in related volcanic rocks has not been well-constrained.

Here, we present, to our knowledge, the first combined Fe and Mg isotopic study of a suite of well-characterized pyroxenite xenoliths from Hannuoba, North China Craton (NCC) (Supplementary Fig. 1). These xenoliths have been interpreted as physical evidence for different episodes of melt injection (Chen et al. 2001; Xu 2002; Fan et al. 2005; Liu et al. 2005, 2010; Hu et al. 2016) and, therefore, provide a unique opportunity to constrain the origins of pyroxenites and to study the influence of mantle metasomatism on generating Fe and Mg isotopic variation in the upper mantle.

Geological setting and petrography of pyroxenite xenoliths

The NCC is a large Archean shield with crustal remnants as old as 3.8 Ga (Liu et al. 1992). It can be divided into three regions: Eastern Block, the Western Block and the

intervening Trans-North China Orogen (Central Orogenic Belt), based on geochronological data, lithological assemblages, tectonic evolution and P–T-t paths (see insert in supplementary Fig. 1) (Zhao et al. 2005). The craton experienced widespread tectonothermal reactivation during the Late Mesozoic and Cenozoic as indicated by the emplacement of voluminous Late Mesozoic granites and extensive Tertiary alkali basalt volcanism (Zhi et al. 1990; Zheng et al. 1998; Fan et al. 2000; Xu 2001; Zhang et al. 2002; Yang et al. 2003; Zhang et al. 2005). Studies of mantle xenoliths and xenocrysts entrained in Paleozoic kimberlites and Cenozoic basalts from the NCC have revealed that the lithosphere beneath the NCC was not only considerably thinned, but also compositionally changed from a Paleozoic cold, thick and refractory lithospheric mantle to a Cenozoic hot, thin and fertile mantle (Griffin et al. 1992, 1998; Menzies et al. 1993, 2007; Menzies and Xu 1998; Fan et al. 2000). Though the idea of lithosphere thinning is widely accepted, the mechanism responsible for such a thinning process still remains hotly debated (Xu 2001; Gao et al. 2004; Zhang et al. 2005; Zheng et al. 2007).

The Hannuoba basalts occur along the northern margin of the Trans-North China Orogen (Supplementary Fig. 1) and comprise an alternating series of alkaline and tholeiitic basalts (Zhi et al. 1990). They have been dated at 14–27 Ma by the K–Ar method (Zhu 1998) and are related to widespread Cenozoic rifting in the NCC (Basu et al. 1991). The alkaline basalts carry a remarkable variety of deep-seated xenoliths from both the lower crust and upper mantle. These xenoliths vary from ultramafic to mafic to felsic with peridotites being dominant, pyroxenites and mafic granulites subordinate and felsic granulites rare. They have been studied to varying extents (Song and Frey 1989; Tatsumoto et al. 1992; Chen et al. 2001; Gao et al. 2002; Xu 2002; Liu et al. 2004, 2005, 2010; Rudnick et al. 2004; Tang et al. 2007; Choi et al. 2008; Zhang et al. 2009b; Zheng et al. 2009; Zhao et al. 2010; Hu et al. 2016).

The xenoliths investigated in this study were collected from the Damaping and Jieshaba localities (Supplementary Fig. 1). They are generally fresh, rounded or ellipsoidal in shape and range from 5 to 20 cm in diameter, with granular to granuloblastic textures and a variable mode (Table 1). They can be divided into three types following the classification of Wilshire and Shervais (1975): (1) Cr-diopside pyroxenites, which are either spinel-bearing or spinel free (Cr-pyroxenites); (2) Al-augite pyroxenites (Al-pyroxenites); and (3) garnet pyroxenites.

The Cr-pyroxenite group includes three websterites and one olivine clinopyroxenite (JSB06-36). They are bright green in hand sample and are texturally well equilibrated (Fig. 1a, b). The Cr-diopside websterites are dominantly composed of clinopyroxene (52–57%) and subordinate orthopyroxene (34–48%), and in some cases, rare spinel and olivine are also present (Table 1). They are characterized by medium- to coarse-grained protogranular texture of clinopyroxene and orthopyroxene, and some websterites exhibit lamellar microstructure with exsolution of orthopyroxene lamella in clinopyroxene (Fig. 1a, b). Olivines are usually anhedral, small (0.3–0.5 mm) and sparse. Spinels occur as small intergranular grains at pyroxene grain boundaries (Fig. 1a, b). Application of the two-pyroxene thermometer of Wells (1977) yields higher equilibration temperatures (1012–1073 °C) for spinel pyroxenites than for the spinel-free pyroxenites (884 °C) (Table 1). There are no discernible differences in temperature between peridotites (839–1072 °C, Chen et al. 2001; Rudnick et al. 2004; Tang et al. 2007; Zhao et al. 2010) and Cr-diopside websterites, indicating a mantle origin for the pyroxenite xenoliths. The olivine clinopyroxenite is mainly composed of clinopyroxene (~56%), with less olivine (~44%) (Table 1, Fig. 1c, d). It is medium- to coarse-grained and exhibits protogranular texture with medium- to coarse-grains of clinopyroxenes (1–3 mm) and medium to small grains of olivine (Table 1, Fig. 1c, d).

The Al-augite pyroxenite group comprises two websterites and one phlogopite clinopyroxenite. The websterites are black in hand sample, are spinel-free and primarily consist of clinopyroxene (54–56%) and orthopyroxene (44–46%). Most websterites show granoblastic texture of medium- to coarse-grained (1–3 mm) (Fig. 1e, f). Both pyroxenes contain exsolution lamellae of the other mineral, implying sub-solidus re- equilibration. These Al-augite websterites yield lower equilibrium temperatures (888–893 °C) than that of Cr-diopside pyroxenites using the two-pyroxene thermometer of Wells (1977). These estimates agree with the estimates reported by Xu (2002) and Chen et al. (2001) for Al-augite pyroxenites from Hannuoba. The phlogopite clinopyroxenite is composed of dominant deep grey (hand specimen) clinopyroxene with about 18% phlogopite and trace amounts of spinel. Phlogopite is anhedral and intergranular (Fig. 1g, h). Spinel in the phlogopite clinopyroxenite is pale greenish, contrasting with its brown colour in the other pyroxenites and is heterogeneously distributed throughout the rock (Fig. 1g, h).

The garnet pyroxenites consist of variable modal proportions of clinopyroxene (usually the major phase), olivine, orthopyroxene, spinel and garnet (Table 1, Fig. 1i–n). They are characterized by medium- to coarse-grained porphyroclastic texture. Garnet often occurs in coronas around spinel, giving rise to classic spinel-cored garnets (Fig. 1i, j). The observation that garnet progressively replaces spinel suggests that garnet was formed at a later stage, at the expense of spinel (Keshav et al. 2007). Garnet may also occur as euhedral and rounded crystals without spinel relicts (Fig. 1k, l). In addition, few samples are composite and

Table 1 Mineral modal abundance (vol.%) and equilibration temperatures (°C) of Hannuoba pyroxenite xenoliths

Sample	Rock type	Texture	Mg#in Cpx	Modal composition (vol.%)						T(Wells) Opx-Cpx	T(BK) Grt-Opx-Cpx	T(NT) Cpx	P(BK) Grt-Opx	P(NG) Grt-Opx
				Ol	Opx	Cpx	Sp	Grt	Phl					
Cr-pyroxenites														
DMP09-02	Websterite	Protogranular	86.9		48	52				884				
DMP09-10	Websterite	Protogranular	90.3	7	34	57	2			1012				
DMP09-22	Websterite	Protogranular	91.3	6	40	52	2			1073				
JSB06-36	Clinopyroxenite	Protogranular	88.6	44		56								
Al-pyroxenites														
DMP09-06	Websterite	Granoblastic	77.5		46	54				888				
DMP09-33	Websterite	Granoblastic	80.1		44	56				893				
DMP09-21	Phl-Clinopyroxenite	Granoblastic	84.9			78	4		18					
Garnet pyroxenites														
JSB06-26	websterite	Granoblastic	91.2	3	23	39	1	34		1077	1080	1081	16.7	19.4
DMP09-38	websterite	Granoblastic	92.4	6	18	32	2	42		1048	1054	1045	19.8	21.1
DMP09-64	websterite	Granoblastic	92.6	12	18	38	1	31		1039	1066	1033	19.8	21.9
JSB09-20	websterite	Granoblastic	89.9	7	14	52	2	25		1059	1076	1063	19.6	21.4
DMP09-13	websterite	Granoblastic	91.7	7	19	38		36		1050	1049	1049	18.0	20.7
DMP09-35	websterite	Granoblastic	89.4	3	5	58	2	32		983	978	931	17.1	16.5
JSB09-05	websterite	Granoblastic	86.4	6	26	34	2	32		1019	1044	1014	18.7	20.7

Ol olivine, *Cpx* clinopyroxene, *Opx* orthopyroxene, *Sp* spinel, *Grt* Garnet, *Phl* Phlogopite

T (wells): Temperature from two-pyroxene thermometer of Wells (1977)

T (BK): Temperature from orthopyroxene-garnet equilibria thermometer of Brey and Köhler (1990)

T (NT): Temperature from single clinopyroxene thermometer of Nimis and Taylor (2000)

P (BK):Orthopyroxene-garnet geobarometer of Brey and Köhler (1990), using the temperature calculated by orthopyroxene-garnet equilibria thermometer of Brey and Köhler (1990)

P (NG):Orthopyroxene-garnet geobarometer of Nickel and Green (1985), using the temperature calculated by thermometer of Wells (1977)

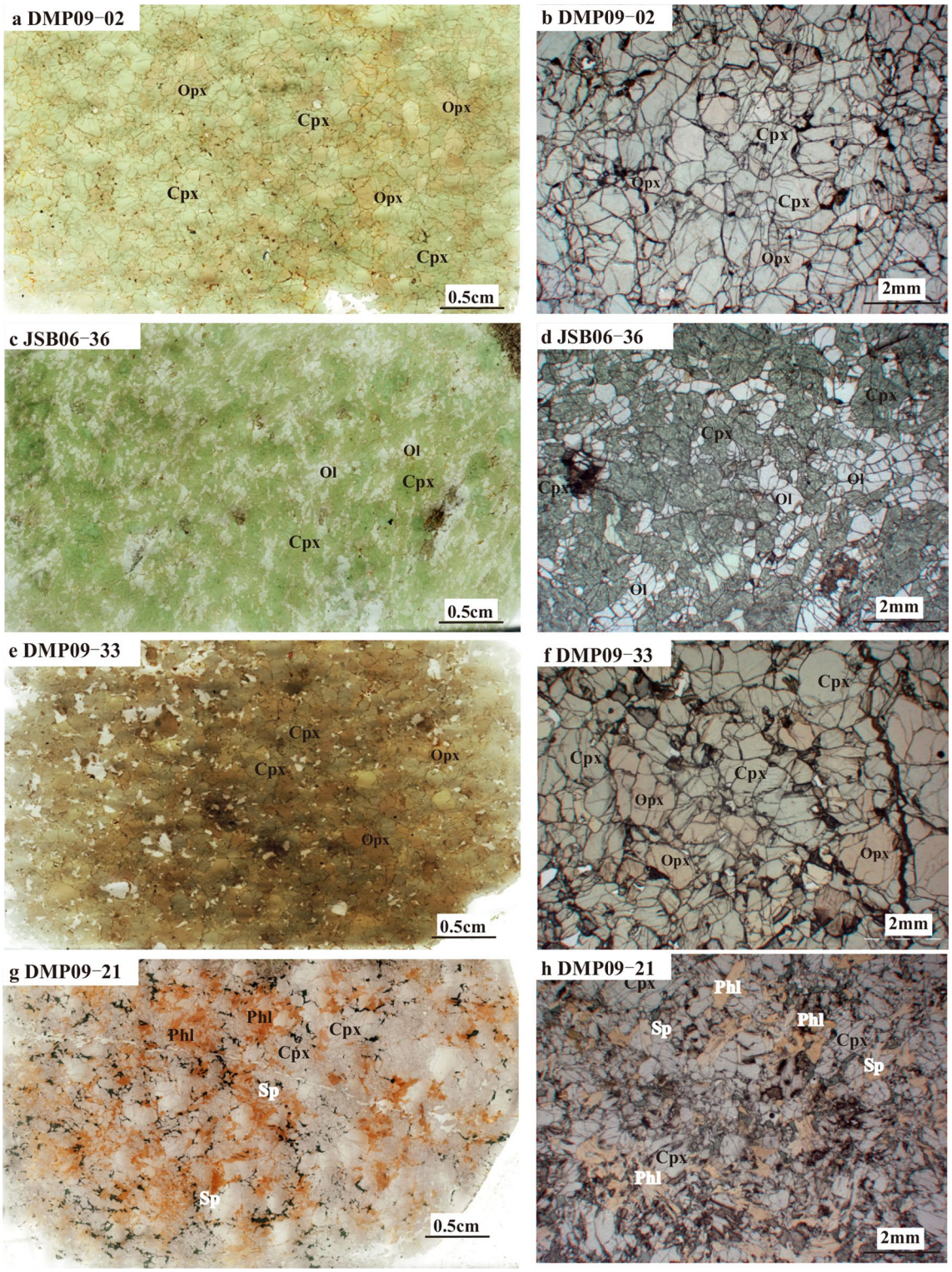

Fig. 1 Thin-section photomicrographs (**a**, **c**, **e**, **i**, **k**, **m**) and representative microphotographs (plane-polarized light) (**b**, **d**, **f**, **h**, **j**, **l**, **n**) of different types of Hannuoba pyroxenite xenoliths

consist of garnet pyroxenite in contact with spinel peridotite (Fig. 1m, n). Garnet grains display dark kelyphitic rims, identical in bulk chemical composition to the primary garnet (Liu et al. 2005). Most garnet pyroxenites equilibrated at 983–1077 °C and 12–16 kbar using the Grt-Opx thermometer of Brey and Köhler (1990) and barometer of

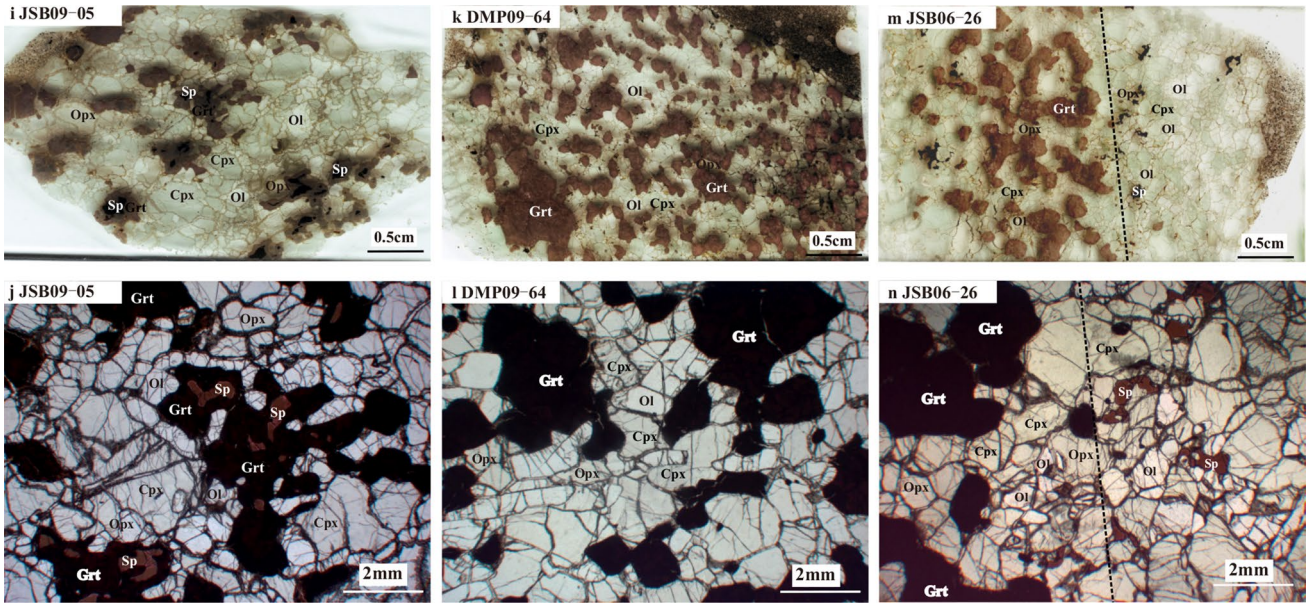

Fig. 1 continued

Nickel and Green (1985), (Table 1), respectively. These estimates are consistent with previous estimates (e.g., Chen et al. 2001; Xu 2002; Liu et al. 2005, 2010; Fan et al. 2005; Hu et al. 2016) and overlap with the T range for Hannuoba spinel peridotites.

Fifteen pyroxenite xenoliths and associated 47 mineral separates were selected for Fe isotopic measurements to cover the wide range of texture and modal/compositional mineralogy of a larger sample collection. Hu et al. (2016) reported Mg isotopic compositions of diverse mantle pyroxenite xenoliths and their separated minerals from Hannuoba. They found that pyroxenite xenoliths from Hannuoba have variable Mg isotopic compositions and mantle metasomatism likely play an important role in producing inter-mineral Mg isotopic disequilibrium and local Mg isotopic variation in the lithospheric mantle. In this study, we analysed five additional pyroxenite xenoliths (two Cr-diopside pyroxenites, two Al-pyroxenites and one garnet pyroxenite) and associated 13 mineral separates from this area for comparison and discussion.

Analytical methods

The xenoliths were cut into slabs and the central parts were used for bulk-rock analyses and for mineral separation. Mineral separates (olivine, orthopyroxene, clinopyroxene, spinel, phlogopite and garnet) were handpicked under a binocular microscope, cleaned with Milli-Q water and dilute hydrochloric acid in an ultrasonic bath and then powdered with an agate mortar in preparation for chemical dissolution.

Major and trace element chemical analysis were conducted at the Institute of Geology and Geophysics, Chinese Academy of Sciences (IGGCAS). Whole-rock major elements were determined by X-ray fluorescence (XRF), mineral major elements were determined by electron microprobe (EPMA), and clinopyroxene trace elements were determined by an inductively coupled plasma mass spectrometer (ICP-MS). More details of the analytical methods can be found in Zhao et al. (2015). The results are given in Supplementary Table 1, 2, 3.

Strontium and Nd isotope analyses of whole rock, including chemical separation and measurements on IsoProbe-T thermal ionization mass spectrometer (GV instruments, England), were performed at IGGCAS. Details of the analytical procedures are similar to those described by Chu et al. (2009). $^{87}Sr/^{86}Sr$ and $^{143}Nd/^{144}Nd$ ratios were corrected for instrumental mass fractionation by normalizing to $^{86}Sr/^{88}Sr = 0.1194$ and $^{146}Nd/^{144}Nd = 0.7219$, respectively. During the period of data collection, the measured values for NBS987-Sr standards was $^{87}Sr/^{86}Sr = 0.710{,}245 \pm 7$ (n = 10), identical to the accepted value 0.710250 and the JNdi-Nd was $^{143}Nd/^{144}Nd = 0.512111 \pm 5$ ($n = 8$), overlapping within error the value of 0.512115 ± 7 (2σ) obtained by Tanaka et al. (2000). BCR-2 yielded $^{143}Nd/^{144}Nd = 0.512674 \pm 13$ (2σ). The procedural blanks were 10, 49, 10 and 19 pg for Rb, Sr, Sm and Nd, respectively, which were less than 0.1% of the amount of samples loaded. The results are given in Supplementary Table 4.

Table 2 Fe isotopic compositions of reference materials, individual minerals and whole rocks of pyroxenite xenoliths from Hannuoba

Sample	Rock type	Mineral	δ^{56}Fe	2SD	δ^{57}Fe	2SD	n	Sample	Rock type	Mineral	δ^{56}Fe	2SD	δ^{57}Fe	2SD	n
BCR-2	Basalt (USGS)	WR	0.07	0.04	0.11	0.07	8	JSB06–26	Grt-websterite	Opx	−0.02	0.02	−0.04	0.05	4
BHVO-2	Basalt (USGS)	WR	0.11	0.03	0.16	0.05	6			Cpx	0.09	0.04	0.08	0.07	4
DMP09-02	Cr-websterite	Opx	−0.04	0.04	−0.04	0.03	4			Sp	0.09	0.02	0.13	0.01	4
		Cpx	0.03	0.02	0.05	0.07	4			Grt	0.20	0.03	0.33	0.08	4
		WR	−0.02	0.05	−0.01	0.07	4			WR	0.10	0.04	0.15	0.07	4
DMP09-10	Cr-websterite	Ol	0.01	0.04	0.02	0.08	3	DMP09-38	Grt-websterite	Ol	−0.16	0.04	−0.24	0.08	4
		Opx	0.02	0.03	0.04	0.04	3			Opx	−0.02	0.01	−0.03	0.07	3
		Cpx	0.04	0.05	0.07	0.05	3			Cpx	−0.03	0.05	−0.07	0.04	4
		Sp	0.13	0.03	0.20	0.06	3			Sp	0.04	0.01	0.07	0.05	4
		WR	0.02	0.04	0.01	0.03	4			Grt	0.20	0.02	0.31	0.08	4
DMP09-22	Cr-websterite	Ol	0.03	0.04	0.04	0.05	4			Grt[a]	0.21	0.04	0.32	0.07	4
		Opx	0.03	0.05	0.01	0.09	4			Average	0.20	0.02	0.31	0.08	8
		Cpx	0.03	0.04	0.04	0.07	7			WR	0.08	0.04	0.12	0.05	4
		Sp	0.12	0.05	0.19	0.08	4	DMP09-13	Grt-websterite	Ol	−0.18	0.05	−0.25	0.07	8
		WR	0.03	0.05	0.03	0.07	4			Opx	0.08	0.03	0.12	0.07	4
JSB06-36	Cr-clinopyroxenite	Ol	−0.01	0.04	−0.02	0.08	7			Cpx	0.10	0.05	0.15	0.08	4
		Cpx	0.08	0.04	0.11	0.06	4			Grt	0.28	0.04	0.42	0.06	4
		WR	0.02	0.05	0.02	0.07	3			WR	0.14	0.05	0.21	0.06	4
DMP09-06	Al-websterite	Opx	0.05	0.04	0.05	0.05	4	JSB09-05	Grt-websterite	Ol	0.05	0.03	0.08	0.05	3
		Cpx	0.07	0.05	0.11	0.08	4			Opx	0.16	0.01	0.25	0.04	3
		WR	0.05	0.05	0.07	0.07	4			Cpx	0.14	0.03	0.21	0.05	3
DMP09-33	Al-websterite	Opx	0.03	0.04	0.04	0.06	3			Sp	0.23	0.02	0.35	0.03	3
		Cpx	0.07	0.02	0.10	0.04	3			Grt	0.27	0.03	0.41	0.04	3
		WR	0.06	0.04	0.09	0.06	6			WR	0.13	0.02	0.20	0.04	7
DMP09-21	Phl-pyroxenite	Cpx	0.67	0.04	1.00	0.09	8	DMP09-35	Grt-websterite	Ol	−0.07	0.04	−0.11	0.04	4
		Phl	0.64	0.05	0.98	0.06	4			Opx	0.03	0.01	0.07	0.06	4
		Phl[a]	0.63	0.02	0.95	0.05	4			Cpx	0.21	0.06	0.31	0.05	10
		Average	0.63	0.02	0.96	0.03	8			Sp	0.32	0.04	0.48	0.06	4
		WR	0.66	0.05	0.99	0.07	8			Gt	0.23	0.06	0.35	0.05	7
JSB06-26	Grt-websterite	Ol	-0.01	0.02	-0.03	0.02	3			WR	0.20	0.04	0.30	0.06	4
Sample	Rock type	Mineral	δ^{56}Fe	2SD	δ^{57}Fe	2SD	n	Sample	Rock type	Mineral	δ^{56}Fe	2SD	δ^{57}Fe	2SD	n
JSB09-20	Grt-websterite	Ol	−0.15	0.02	−0.22	0.07	3	JSB09-20	Grt-websterite	Grt	0.21	0.05	0.32	0.06	3
		Opx	0.08	0.04	0.12	0.06	3			WR	0.13	0.02	0.19	0.06	4
		Cpx	0.11	0.03	0.17	0.06	3	DMP09-64	Grt-websterite	WR	0.14	0.02	0.21	0.04	4
		Sp	0.18	0.04	0.27	0.07	3								

WR whole rock, *Ol* olvine, *Opx* orthopyroxene, *Cpx* clinopyroxene, *Spl* spinel, *Grt* Garnet, *Phl* phlogopite

[a] Re-analysis from chemical separation to isotopic analysis, starting from the new digestion of same sample powder

Table 3 Mg isotope compositions of pyroxenites and their minerals from Hannuoba

Sample	Rock type	Mineral	δ^{26}Mg	2SD	δ^{25}Mg	2SD	N
BCR-2	Basalt (USGS)	WR	−0.23	0.04	−0.11	0.02	10
BHVO-2	Basalt (USGS)	WR	−0.26	0.03	−0.13	0.02	3
DMP09-02	Cr-websterite	Opx	−0.29	0.04	−0.14	0.01	3
		Cpx	−0.25	0.03	−0.13	0.02	3
		WR	−0.28	0.04	−0.14	0.03	3
JSB06-36	Cr-clinopyroxenite	Ol	−0.26	0.04	−0.13	0.01	3
		Cpx	-0.23	0.04	-0.11	0.01	3
		WR	−0.25	0.04	−0.13	0.04	3
DMP09-06	Al-websterite	Opx	−0.28	0.05	−0.14	0.03	3
		Cpx	−0.22	0.03	−0.11	0.02	3
		WR	−0.26	0.05	−0.13	0.02	3
JSB09-05	Garnet-websterite	Ol	−0.35	0.02	−0.17	0.03	3
		Opx	−0.35	0.03	−0.17	0.02	3
		Cpx	−0.34	0.04	−0.17	0.02	3
		Sp	0.04	0.03	0.02	0.02	3
		Grt	−0.68	0.03	−0.34	0.01	3
		WR	−0.43	0.04	−0.21	0.02	3
DMP09-21	Phl-pyroxenite	Cpx	−1.54	0.04	−0.77	0.03	3
		Phl	−1.50	0.03	−0.75	0.03	3
		Phl[a]	−1.50	0.03	−0.75	0.01	6
		Average	−1.50	0.01	−0.75	0.01	9
		WR	−1.53	0.04	−0.77	0.03	3

WR whole rock, *Ol* olvine, *Opx* orthopyroxene, *Cpx* clinopyroxene, *Spl* spinel, *Grt* Garnet, *Phl* phlogopite

[a] Re-analysis from chemical separation to isotopic analysis, starting from the new digestion of same sample powder

Fe and Mg isotopic ratios were measured at the Chinese Academy of Sciences Key Laboratory of Crust-Mantle Materials and Environments, University of Science and Technology of China (USTC). Detailed analytical procedures, including sample dissolution, column chemistry and instrumental analysis, are similar to that reported in Huang et al. (2011); An et al. (2014); Li et al. (2016a). Approximately 2–20 mg of 200 mesh whole rock or mineral (olivine, orthopyroxene, clinopyroxene, garnet and phlogopite) powders were dissolved using 5:1 mixtures of concentrated HF and HNO_3 in 15 ml Teflon beakers on a hot plate at 120 °C while spinels were dissolved using a mixture of 1:1 HF and HCl in 5 ml steel-jacketed bomb in an oven at 180 °C for a week. After complete dissolution, the final solution was treated with concentrated HCl repeatedly to convert the cations into chlorides. At least two reference materials were processed as unknown samples for each batch of column chemistry to access accuracy and reproducibility. For some samples, replicate analyses on different aliquots were performed where there was adequate powdered material.

Iron was purified on an anion exchange resin (Bio-Rad AG1-X8, 200-400 mesh) in HCl using established procedures (Huang et al. 2011; Li et al. 2016a). The Fe isotopic composition was obtained using the sample-standard bracketing method on a Thermo-Finnigan Neptune MC-ICP-MS in medium-resolution mode (Huang et al. 2011; Li et al. 2016a). Iron isotope data are reported in standard δ notation in per mil relative to reference material IRMM-014: $\delta^{X}Fe = [(\delta^{X}Fe/^{54}Fe)_{sample}/(\delta^{X}Fe/^{54}Fe)_{IRMM\text{-}014} - 1] \times 1000$, where X refers 57 or 56. ^{53}Cr, ^{54}Fe, ^{56}Fe, ^{57}Fe, ^{58}Fe, and ^{60} Ni were measured in a static mode on the L3, L1, H1, H2, and H4 Faraday cups, respectively. The total procedural blank was <10 ng and is negligible compared to Fe loaded on the column (~50 μg of Fe). The long-term external reproducibility of the ^{56}Fe/^{54}Fe ratio measurements at medium -resolution modes is better than 0.05‰ amu^{-1} at the 2SD level based on replicate measurements of in-house GSB Fe and UI Fe solutions against IRMM-014. Two USGS standards, BHVO-2 and BCR-2, yield average δ^{57}Fe values of 0.16 ± 0.05 (2SD; $n = 6$) and 0.11 ± 0.07 (2SD; $n = 8$), respectively. Our values for these rock standards are identical to the values (δ^{57}Fe = 0.17 ± 0.02 for BHVO-2 and δ^{57}Fe = 0.13 ± 0.01 for BCR-2) recommended by Craddock and Dauphas (2011) and references therein when the equivalent 2 SD errors are considered. Duplicate δ^{57}Fe analyses of DMP09-21 clinopyroxene

from two sample aliquots also show good reproducibility (1.00 ± 0.09 vs. 1.00 ± 0.05).

Approximately 0.5 ml aliquots of the stock bulk solution were dried down, evaporated with concentrated HNO_3, and then dissolved in 0.5 ml 1 N HNO_3 for chromatographic separation. Magnesium purification was achieved by cation exchange chromatography with Bio-Rad AG50 W-X12 (200–400 mesh) resin followed the established procedure of An et al. (2014). Ultrapure reagents were used for all steps, and the total procedural blank was <10 ng, which is insignificant relative to the amount of Mg processed through the whole chemical procedure (~30 μg). Purified Mg sample solutions (~2 ppm Mg in 2% HNO_3) were introduced into the "wet" plasma using a quartz dual cyclonic-spray chamber and an ESI 50 μL/min PFA Teflon nebulizer. Samples were analysed using the Neptune MC-ICPMS in medium-resolution mode with ^{24}Mg, ^{25}Mg, and ^{26}Mg detected on the L3, C, and H3 Faraday cups simultaneously. Runs of sample and standard were separated by washes using 3% HNO_3 for 2 min to avoid cross-contamination. Magnesium isotope data are reported in standard δ notation in per mil relative to reference material DSM3 (Galy et al. 2003), defined as $\delta^{X}Mg = [(^{X}Mg/^{24}Mg)_{sample}/(^{X}Mg/^{24}Mg)_{DSM3} - 1] \times 1000$, where X is either 25 or 26. The long-term external precision was evaluated by analysis of international Mg solution standards and rock standards and is generally better than ±0.05 for $\delta^{26}Mg$ (An et al. 2014). Analyses of the well-characterized USGS Mg rock standards in this study yield $\delta^{26}Mg = -0.26 \pm 0.03$ (2SD, $n = 3$) for BHVO-2, and -0.23 ± 0.03 (2SD, $n = 10$) for BCR-2, respectively (Table 3), which are in excellent agreement with the recommended values within error ($\delta^{26}Mg = -0.24 \pm 0.08$ for BHVO-2 and $\delta^{26}Mg = -0.27 \pm 0.02$ for BCR-2; Teng et al. 2017 and references therein). One sample (phlogopite from DMP09-21) analysed in duplicate on separate aliquots and the Mg isotopic composition shows good reproducibility (Table 3).

Results

Whole-rock chemistry

Major element abundance for pyroxenites is given in Supplementary Table 2 and illustrated in Fig. 2. Available data for Hannuoba basalts, pyroxenites and peridotites from previous studies are also shown for comparison. As seen in Fig. 2, Hannuoba pyroxenites exhibit a much wider range in composition compared with Hannuoba peridotites, reflecting their more varied mineralogy. The whole-rock mg-numbers [Mg# = 100 × atomic Mg/(Mg + Fe^{2+})] for Cr-diopside pyroxenites range from 87.6 to 91.5, while the Al-augite pyroxenites have significantly lower values (76.3–83.3). Both Cr-diopside pyroxenites and Al-augite pyroxenites have higher Al_2O_3, CaO and SiO_2 contents compared to the peridotites (Fig. 2a–c); however, they have lower Ni concentrations than the peridotites (Fig. 2d). The garnet pyroxenites differ from the Cr-diopside pyroxenites and Al-augite pyroxenites in having significantly higher K_2O, Al_2O_3 and Ni contents with Mg#s range from 84.7 to 90.6 (Fig. 2, Supplementary Table 1). The phlogopite clinopyroxenite has the highest Al_2O_3, CaO and TiO_2 but the lowest Ni contents among the samples studied in this work (Fig. 2a–c). The major element compositions of Hannuoba pyroxenites plot off the extension trends between the Hannuoba peridotites and calculated equilibrium melts (Fig. 2a, b), arguing against their origin as in situ melting products of the host peridotites. All the pyroxenites have higher MgO and Ni concentrations than those of Hannuoba basalts, including MORB (Fig. 2).

Mineral compositions

Olivine

Olivines from Cr-diopside pyroxenites generally have homogeneous major element compositions (Supplementary Table 3). The olivines in two websterite xenoliths have restricted Fo (89.0–90.8) and NiO (0.37–0.40 wt.%) contents (Supplementary Table 2, Supplementary Fig. 2a), approaching the composition of olivines from mantle peridotitic xenoliths entrained in Hannuoba Cenozoic basalts (Supplementary Fig. 2a). Olivine in the olivine clinopyroxenite (JSB06-36) has lower Fo (87.2) and NiO contents (0.15 wt. %) than the olivines of the Cr-diopside websterites (Supplementary Table 2, Supplementary Fig. 2a).

Olivines in the garnet pyroxenite xenoliths display large compositional variations with Fo ranging from 86.1 to 91.2, which partly overlaps values in the Hannuoba peridotites (Supplementary Fig. 2a). Olivine in JSB09-20 is heterogeneous, with Mg# = 90.0 in the cores of grains and Mg# = 86.7 in the rims (Supplementary Table 2). CaO contents for olivines of both Cr-diopside pyroxenites and garnet pyroxenites are low (0.04–0.11 wt. %) and similar to those estimated (CaO: 0.05–0.1 wt. %) by Brey and Köhler (1990) for rocks of mantle origin.

Orthopyroxene

Orthopyroxenes are broadly homogeneous with no compositional zonation. Orthopyroxenes in the Cr-diopside pyroxenites are chromian enstatite, which have high Mg# of 85.2–91.2 and Al_2O_3 contents of 4.3–5.5 wt%. Their Cr_2O_3 content varies from 0.59 to 0.60 wt% (Supplementary Table 2, Supplementary Fig. 2b). Orthopyroxene in the Al-augite pyroxenites is Al-rich enstatite (En

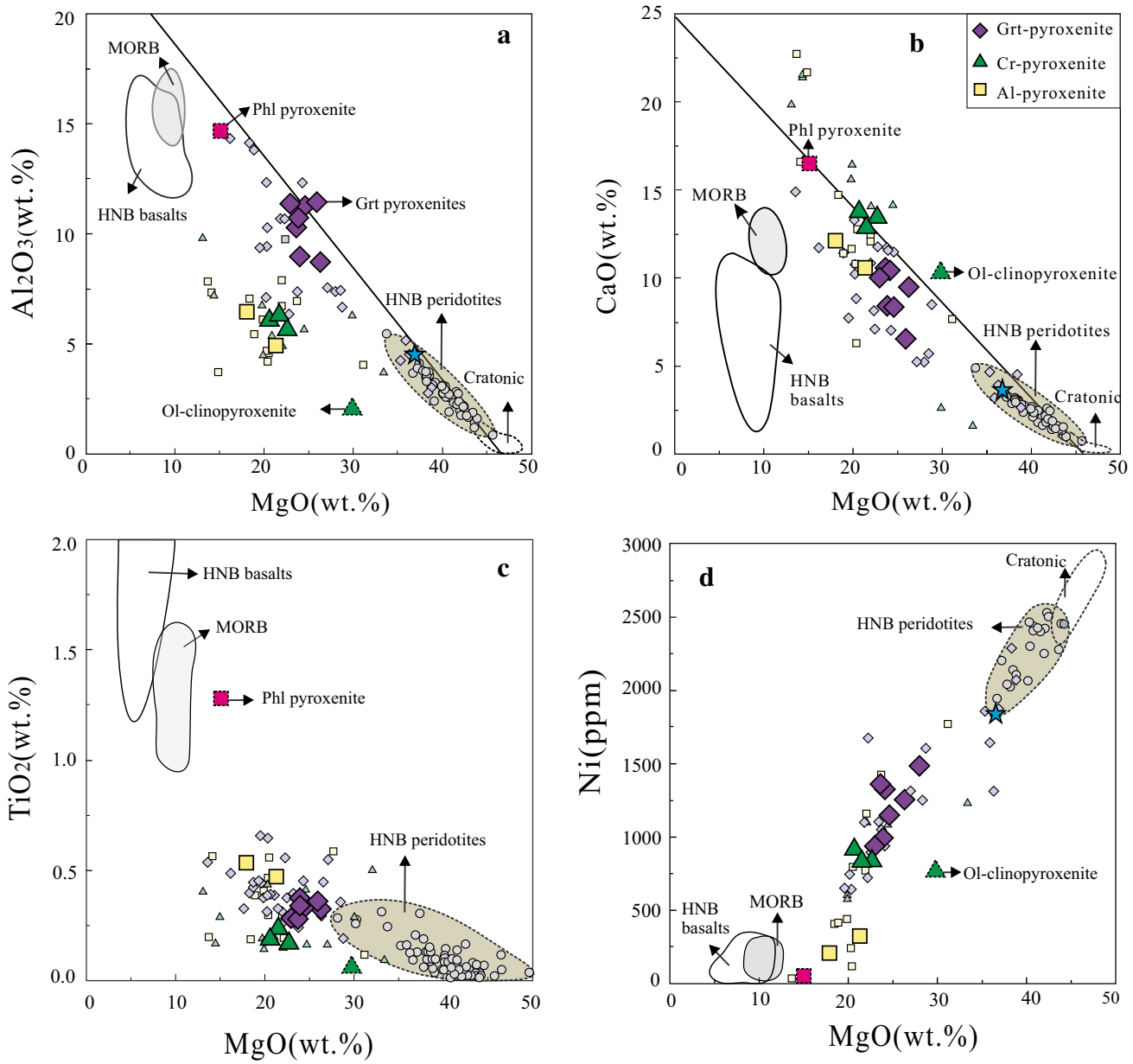

Fig. 2 Plots of whole-rock MgO against Al_2O_3 (**a**), CaO (**b**), TiO_2 (**c**) and Ni (**d**) for the Hannuoba pyroxenite xenoliths. The smaller symbols represent data from the literature. Data for Hannuoba peridotites (Song and Frey 1989; Chen et al. 2001; Rudnick et al. 2004; Fan et al. 2005; Choi et al. 2008; Zhang et al. 2009b) and pyroxenites (Chen et al. 2001; Xu 2002; Fan et al. 2005; Liu et al. 2005; Hu et al. 2016) are plotted for comparison. The star denotes the composition of primitive mantle from McDonough and Sun (1995). *Solid line* represents an "extraction" line between the Hannuoba peridotites as a residue and calculated equilibrium melt taken from Xu (2002). The *grey dashed lines* represent the compositional fields of typical cratonic peridotites defined by Tanzanian xenoliths (Lee and Rudnick 1999). The data for Hannuoba basalts are from Zhi et al. (1990); Basu et al. (1991); Fan and Hooper (1991); Liu et al. (1994); Qian et al. (2015); Hu et al. (2016). The fields of mid-ocean ridge basalt (MORB) in **a** and **b** are from Downes (2007) with data from Melson et al. (1976), Schilling et al. (1983); Korenaga and Kelemen (2000), in c is from Bodinier and Godard (2014) with data from the PetDB database, and in **d** is from Yu et al. (2010) with data from Jacob (2004). Major element data of Hannuoba pyroxenite xenoliths are from supplementary Table 1

72.2–76.1; Supplementary Table 2) with a Mg# of 73.0–76.9. They have much lower CaO (0.46–0.53 wt%) and Cr_2O_3 (0.13–0.16 wt%) contents, but distinctly higher contents of MnO (0.25–0.27 wt%) when compared to Cr-diopside pyroxenites (Supplementary Table 2, Supplementary Fig. 2b). Orthopyroxenes in the garnet pyroxenites have relatively higher Mg# (86.7–91.3), CaO (0.89–1.08 wt%) and Cr_2O_3 (0.18–0.48 wt%) and lower

MnO (0.12–0.14 wt%) contents compared to those in the Al-augite pyroxenites and fall within the trend for the Hannuoba peridotite on a Mg# versus Cr_2O_3 plot (Supplementary Table 2, Supplementary Fig. 2b).

Clinopyroxene

Clinopyroxenes from the Cr-diopside pyroxenites have no compositional zonation. Their compositions ($En_{44.4–49.3}Wo_{44.1–50.7}Fs_{4.8–6.7}$) fall within the diopside field on a Wo–En–Fs diagram (Morimoto 1988). They are characterized by Mg# values of 86.9–91.3, higher than those of coexisting orthopyroxenes and olivines (Supplementary Table 2). Clinopyroxene from the olivine clinopyroxenite (JSB06-36) contains lower Al_2O_3 (2.99 wt%) and TiO_2 (0.06 wt%) and higher Na_2O (1.77 wt%) than the Cr-diopside websterites (3.14–4.9 wt% Al_2O_3, 0.19–0.32 wt% TiO_2, 0.92–1.13 wt% Na_2O) (Supplementary Table 2, Supplementary Fig. 2b).

Clinopyroxenes from the Al-augite pyroxenites are Cr-poor augites or diopsides with Mg# ranging from 77.5 to 84.9 (Supplementary Fig. 2). They have high Al_2O_3 (5.3–9.1 wt%) and low Na_2O (0.39–0.88 wt%) contents and Cr_2O_3 is usually below 0.3 wt%. They have a much higher TiO_2 (0.74–0.81 wt%) content than the clinopyroxenes from Cr-diopside pyroxenites (Supplementary Table 2, Supplementary Fig. 2b).

Clinopyroxenes from garnet pyroxenites are all diopside with Mg# ranging from 86.9 to 91.3 (Supplementary Table 2, Supplementary Fig. 2b). They have high Al_2O_3 (5.00–8.34 wt%), low to moderate TiO_2 (0.34–0.64 wt%) and Na_2O (0.58–1.96 wt%) contents (Supplementary Table 2, Supplementary Fig. 2b).

Spinel

Spinels in the Cr-diopside pyroxenites have high Mg# (72.9–75.0), typical of mantle spinels. Their Cr# [100 × Cr/(Cr + Al)] is in the range of 19.1–21.6, much lower than the Cr# of on-craton spinels (40–91, Griffin et al. 1998) but similar to that of off-craton spinels (11–23, Zheng et al. 2006). For the Al-augite pyroxenites, spinel only occurs in the phlogopite clinopyroxenite (DMP09-21). The green spinel in this phlogopite clinopyroxenite is characterized by much lower Cr# (0.2) and NiO (0.03 wt%) and higher Al_2O_3 contents (63.5 wt. %) with a lower Mg# (65.8) than spinels from the Cr-diopside pyroxenites and garnet pyroxenites (Supplementary Table 2, Supplementary Fig. 2b). Spinels from the garnet pyroxenites analysed here are Cr-poor and Al-rich, with moderate Mg# (71.3–80.5). Their Cr# values (1.4–14.4) are lower than those from Cr-diopside pyroxenites (Cr# = 19.1–21.6).

Garnet

All the garnets investigated display dark kelyphitic rims. However, these kelyphites possess an almost identical bulk chemical composition to the primary garnet, with only a few analyses yielding higher contents of Na_2O, suggesting alkali ingress from metasomatic melts (Liu et al. 2010). In garnet pyroxenites, garnets are pyrope-rich (pyrope $_{67.5–82.2}$, almandine $_{3.0–20.2}$, grossular $_{12.2–15.5}$), consistent with their relatively high Mg# (71.3–80.3) and mantle origin. Their CaO and Cr_2O_3 contents fall within the websteritic field (Sobolev et al. 1973) (Supplementary Fig. 2d).

Phlogopite

The composition of phlogopite in the phlogopite clinopyroxenite is relatively homogeneous with high Mg# (89.5), high K_2O (9.03 wt. %) and TiO_2 (3.52 wt. %). The Mg# of the phlogopite is much higher than that in coexisting clinopyroxene (Mg# = 84.9, Supplementary Table 2), indicating the minerals are not in chemical equilibrium.

Trace elements

Whole rock trace element data and REE contents in clinopyroxene and garnet are given in Supplementary Table 3 and illustrated in Supplementary Fig. 3. Pyroxenite xenoliths from Hannuoba have higher rare earth element (REE) contents than the residual spinel peridotites reported in the literature (Supplementary Fig. 3). For Cr-diopside pyroxenite and Al-augite pyroxenite samples, clinopyroxene REE patterns resemble those in bulk whole-rocks but absolute REE concentrations are higher in the former (Supplementary Fig. 3), suggesting that clinopyroxenes are the dominant reservoir of REE for these two pyroxenites groups. Clinopyroxenes from Cr-diopside pyroxenites exhibit substantial variation in both absolute concentrations of trace elements (ΣREE = 14–104 ppm) and diversity of chondrite-normalized REE pattern (Supplementary Table 3, Supplementary Fig. 3). Both LREE-depleted and LREE-enriched patterns are observed in Cr-diopside pyroxenites (Supplementary Fig. 3). Clinopyroxene in the olivine clinopyroxenite (JSB06-36) has a higher REE abundance than other Cr-diopside pyroxenites and exhibits a convex-upward REE pattern (Supplementary Fig. 3). In a primitive mantle-normalized spider diagram (Supplementary Fig. 3), the clinopyroxenes in all Cr-diopside pyroxenites show obvious negative anomalies in HFSE (Nb, Ta, Zr, Hf) and positive anomalies in U and Sr.

Clinopyroxenes from two Al-augite websterites exhibit uniform convex-upward REE patterns with an apex at Sm, typical of pyroxenite xenoliths in alkali basalts (McDonough and Frey 1989). In a primitive mantle-normalized spider diagram (Supplementary Fig. 3), Al-augite pyroxenites have pronounced negative HFSE (Nb, Ta, Zr and Hf) anomalies and very low Rb and Ba contents. The phlogopite clinopyroxenite (DMP09-21) is distinguished from other Al-augite pyroxenites by a higher REE abundance and Rb, Ba, Th, U enrichment (Supplementary Fig. 3).

In contrast, the REE are distributed between garnet and pyroxene in garnet pyroxenites and, therefore, the clinopyroxene REE pattern does not mirror that of the whole-rock (Supplementary Fig. 3). LREE-depleted, LREE-enriched and essentially flat patterns are observed in various garnet pyroxenites (Supplementary Fig. 3). The flat pattern of some garnet pyroxenites is simply a consequence of abundant modal garnet. All garnet pyroxenites are characterized by positive Sr anomalies and no Eu anomaly (Supplementary Fig. 3). All clinopyroxenes from garnet pyroxenites are LREE enriched but have lower HREE contents, indicating equilibration with garnet. REE patterns in garnet from garnet pyroxenites display significant LREE depletion and MREE to HREE enrichment, with no Eu anomaly (Supplementary Fig. 3).

Sr and Nd isotopic compositions

The Sr and Nd isotopic compositions for Hannuoba pyroxenites are given in Supplementary Table 4 and illustrated in Supplementary Fig. 4. The data for peridotite xenoliths (Song and Frey 1989; Tatsumoto et al. 1992; Choi et al. 2008; Zhang et al. 2009b) and a range of basalts (Song et al. 1990; Basu et al. 1991) are also shown for comparison. The Sr and Nd isotopic ratios have been corrected for radioactive decay to 135 Ma, which is the approximate age of most pyroxenites (Xu 2002).

Cr-diopside pyroxenites display variable isotopic ratios: $^{87}Sr/^{86}Sr = 0.703335–0.705329$ and $^{143}Nd/^{144}Nd = 0.512597–0.513079$ ($\varepsilon_{Nd} = -1.1$ to $+9.2$). In the Sr–Nd isotope diagram (Supplementary Fig. 4), the Sr and Nd isotopic compositions plot within the field of data reported previously for the Hannuoba Cr-diopside series pyroxenites (Song and Frey 1989; Tatsumoto et al. 1992; Xu 2002), which form a linear trend along the Sr–Nd mantle array, and also overlap with the field for Hannuoba peridotites (Supplementary Fig. 4). Al-augite pyroxenites are isotopically distinct, with higher Sr ($^{87}Sr/^{86}Sr = 0.706382–0.710140$) and unradiogenic Nd ($^{143}Nd/^{144}Nd = 0.511775–0.511866$; $\varepsilon_{Nd} = -14.9$ to -16.8). These Sr and Nd isotopic compositions plot outside the isotopic compositional range defined by oceanic basalts and fall in the granulite area (Supplementary Fig. 4).

Garnet pyroxenites have the following isotopic compositions: $^{87}Sr/^{86}Sr = 0.703940–0.707731$ and $^{143}Nd/^{144}Nd = 0.512880–0.513066$ ($\varepsilon Nd = +5.3$ to $+7.4$). These isotopic compositions largely overlap with the ranges of Sr–Nd data obtained by Xu (2002) on a different set of garnet pyroxenites (Supplementary Fig. 4). They have relatively high $^{87}Sr/^{86}Sr$ ratios at given εNd relative to the general trend defined by Hannuoba Cr-diopside pyroxenites and two Al-augite pyroxenites.

Iron isotopes

Fe isotopic compositions of reference materials, individual minerals and pyroxenite xenolith whole rocks from Hannuoba are presented in Table 2 and plotted in Fig. 3.

Cr-diopside pyroxenites and Al-augite pyroxenites

With the exception of one phlogopite clinopyroxenite, the four Hannuoba Cr-diopside pyroxenites and two Al-augite pyroxenites define a narrow Fe isotopic variation ($\delta^{57}Fe = -0.01$ to 0.09) with an average of 0.03 ± 0.08 (2SD, $n = 6$) (Table 2, Fig. 3). These values mainly fall within the range reported previously for Hannuoba peridotite xenoliths within error ($\delta^{57}Fe = -0.19$ to 0.08; Zhao et al. 2010) but fall significantly below the value of oceanic basalts (0.15 ± 0.01, $2SD/\sqrt{n}$, $n = 234$) (Poitrasson et al. 2004; Schoenberg and Blanckenburg 2006; Weyer and Ionov 2007; Teng et al. 2008, 2013; Williams and Bizimis 2014; Konter et al. 2016).

Similar to whole rocks, the mineral separates from both the Cr-diopside pyroxenites and Al-augite pyroxenites also display a narrow range of Fe isotopic variations (Table 2, Fig. 3). The $\delta^{57}Fe$ values range from -0.02 to 0.04 in the olivines, -0.04 to 0.05 in the orthopyroxenes, 0.04 to 0.11 in the clinopyroxenes and 0.19 to 0.20 in the spinels. The average mineral $\delta^{57}Fe$ values (based on all analyses) is 0.01 ± 0.06 ($n = 3$, 2SD) for olivine, 0.02 ± 0.08 ($n = 5$, 2SD) for orthopyroxene, 0.08 ± 0.07 ($n = 6$, 2SD) for clinopyroxenes and 0.19 ± 0.02 for spinels ($n = 2$, 2SD). The order of $^{57}Fe/^{54}Fe$ for constituent minerals from the Cr-diopside pyroxenites and Al-augite pyroxenites is $\delta^{57}Fe_{Spl} > \delta^{57}Fe_{Cpx} > \delta^{57}Fe_{Opx} \geq \delta^{57}Fe_{Ol}$ (Table 3, Fig. 3).

It is noted that the phlogopite clinopyroxenite (DMP09-21) yields $\delta^{57}Fe$ values of 0.99, which are the heaviest found in this study or reported in the literature for mantle rocks. Clinopyroxene and phlogopite from the phlogopite clinopyroxenite also have much heavier Fe isotopic compositions ($\delta^{57}Fe = 1.00$ and $\delta^{57}Fe = 0.95$, respectively) than typical mantle clinopyroxene and phlogopite. These values are, however, consistent with the corresponding extremely heavy whole-rock $\delta^{57}Fe$ values (Table 3, Fig. 3).

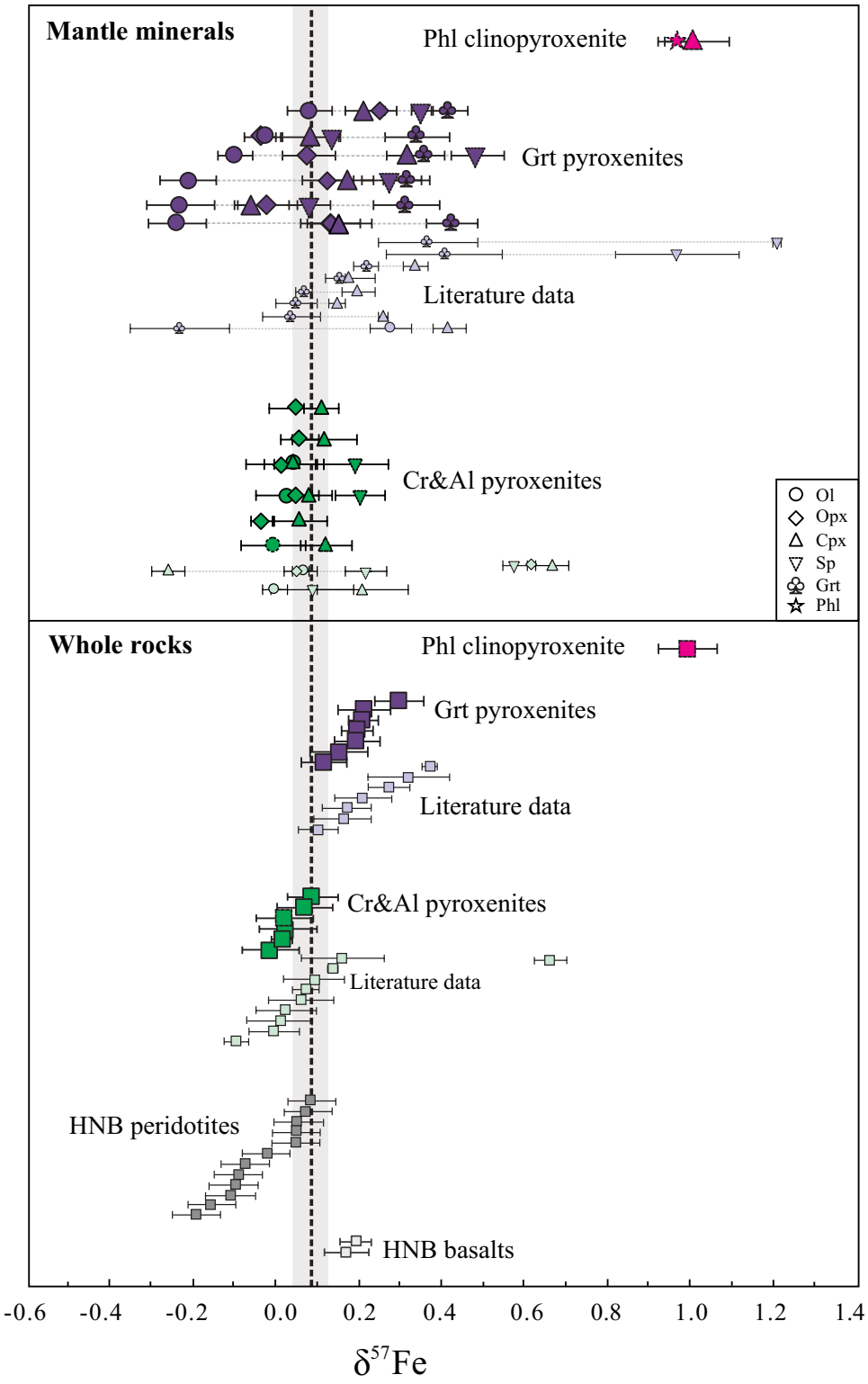

Fig. 3 Comparison of Fe isotopic data for the Hannuoba pyroxenite xenoliths and their associated minerals with published peridotite data (Williams et al. 2005, 2014; Schoenberg and Blanckenburg 2006; Zhao et al. 2010; Poitrasson et al. 2013; Craddock and Dauphas 2011; Macris et al. 2015). The *smaller symbols* represent data from the literature. The *dash vertical line* and *grey band* at $\delta^{57}Fe = 0.09 \pm 0.04$ is the fertile upper-mantle value inferred peridotites without evidence of previous melt depletion and metasomatism from Yangyuan, NCC (Zhao et al. 2015). Data are from Table 2. *Error bars* are 2 SD

Garnet-bearing pyroxenites

Compared to Cr-diopside pyroxenites and Al-augite pyroxenites, seven garnet-bearing pyroxenites have variable Fe isotopic compositions ($\delta^{57}Fe = 0.12$–0.30), with an average of $\delta^{57}Fe = 0.20 \pm 0.11$ ($n = 7$, 2SD), which is distinctly heavier than the average $\delta^{57}Fe$ values of the Hannuoba peridotite xenoliths, Cr-diopside pyroxenites and

Al-augite pyroxenites (Fig. 3), but indistinguishable δ^{57}Fe values for the Hannuoba basalts (0.18 ± 0.03, 2SD, $n = 2$; Zhao et al. 2012) and oceanic basalts (0.15 ± 0.01, 2SD/$\sqrt{n}$, $n = 234$) (Poitrasson et al. 2004; Schoenberg and Blanckenburg 2006; Weyer and Ionov 2007; Teng et al. 2008, 2013; Williams and Bizimis 2014; Konter et al. 2016). Relative to minerals from the Cr-diopside pyroxenites and Al-augite pyroxenites, the δ^{57}Fe values for the minerals separated from the Hannuoba garnet-bearing pyroxenites also display larger variations: −0.25 to 0.08, −0.04 to 0.25, −0.07 to 0.31, 0.07 to 0.48 and 0.31 to 0.42 for olivine, orthopyroxene, clinopyroxene, spinel and garnet, respectively (Table 2, Fig. 3). Overall, the order of ^{57}Fe/^{54}Fe values for constituent minerals from the garnet-bearing pyroxenites is $\delta^{57}Fe_{Grt} > \delta^{57}Fe_{Spl} > \delta^{57}Fe_{Cpx} > \delta^{57}Fe_{Opx} > \delta^{57}Fe_{Ol}$ (Table 2 and Fig. 3).

Magnesium isotopes

Magnesium isotopic compositions of reference materials, five whole-rock samples and 13 mineral separates are reported in Table 3 and plotted in Fig. 4.

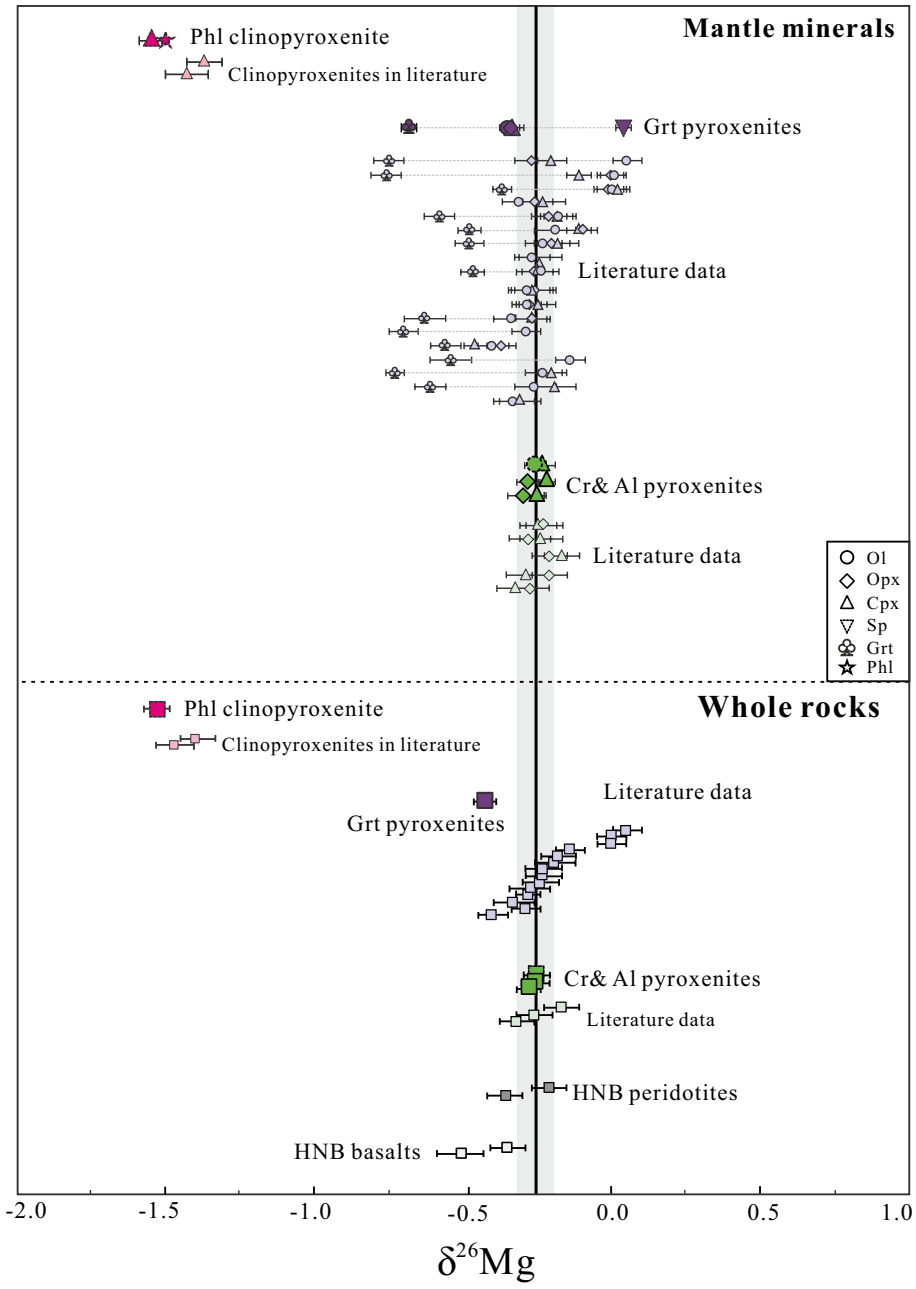

Fig. 4 Compilation of Mg isotopic data for the Hannuoba pyroxenite xenoliths and mineral separates with published pyroxenite data (Hu et al. 2016). The *smaller symbols* represent data from the literature. The *solid vertical line* and *grey band* at $\delta^{26}Mg = -0.25 \pm 0.07$ is the mantle value (Teng et al. 2010). Data are from Table 3. *Error bars* are 2 SD

Whole rocks

The δ^{26}Mg values of five pyroxenite whole rocks vary from −1.53 to −0.25 (Table 3, Fig. 4). Both the Cr-diopside pyroxenites and Al-augite pyroxenites display a limited range (−0.28 to −0.25 with an average of −0.26 ± 0.03 (2 SD, $n = 3$)), consistent with values previously reported for the Hannuoba Cr-diopside pyroxenites and Al-augite pyroxenites (Hu et al. 2016; Fig. 4), and the estimated δ^{26}Mg value of the mantle (−0.25 ± 0.07, 2SD; Teng et al. 2010).

In contrast, the garnet-bearing pyroxenite xenolith has a light Mg isotopic composition (δ^{26}Mg = − 0.43 ± 0.04, 2SD) relative to the mantle (Fig. 4) and falls into the range reported for the Hannuoba garnet-bearing pyroxenites (−0.48 to −0.10; Hu et al. 2016). The most surprising result is that the phlogopite clinopyroxenite (DMP09-21) shows a significantly light Mg isotope signature (δ^{26}Mg = −1.53), which is the lightest δ^{26}Mg value determined in this study (Table 3, Fig. 4).

Mineral separates

Olivines and pyroxenes from the Hannuoba Cr-diopside pyroxenites and Al-augite pyroxenites also have mantle-like δ^{26}Mg values (Table 3, Fig. 4) with δ^{26}Mg ranging from −0.29 to −0.28 in orthopyroxenes, and −0.25 to −0.22 in clinopyroxenes. Olivine from the Cr-diopside pyroxenites has a δ^{26}Mg of −0.26 ± 0.04 (2SD) (Fig. 4). These new data are in agreement with those previously reported for these minerals from Hannuoba Cr-diopside pyroxenites and Al-augite pyroxenites (average δ^{26}Mg = −0.25; Hu et al. 2016; Table 3, Fig. 4). The order of ^{26}Mg/^{24}Mg for constituent minerals from the Cr-diopside pyroxenites and Al-augite pyroxenites is $\delta^{26}Mg_{Cpx} \geq \delta^{26}Mg_{Opx} = \delta^{26}Mg_{Ol}$ (Table 3, Fig. 4).

In contrast to the Hannuoba Cr-diopside pyroxenites and Al-augite pyroxenites, the mineral separates in the garnet-bearing pyroxenite span a total δ^{26}Mg range of 0.72‰, from −0.68 in garnet to 0.04 in spinel, in agreement with the data reported by Hu et al. (2016). Garnet yields an isotope composition of −0.68 in δ^{26}Mg, which is systematically lighter than co-existing olivine and pyroxene (Fig. 4). Coexisting olivine and pyroxenes in the garnet-bearing pyroxenite are isotopically irresolvable in δ^{26}Mg within analytical uncertainty (−0.35 for olivine, −0.35 for orthopyroxene, and −0.34 for clinopyroxene, respectively) and slightly lighter than the mantle Mg isotopic composition. The Mg isotopic composition of spinel (δ^{26}Mg = 0.04) from this garnet-bearing pyroxenite is significantly heavier than those of coexisting silicate minerals (Table 3, Fig. 4). The ^{26}Mg/^{24}Mg of constituent minerals from this garnet-bearing pyroxenite resolves as $\delta^{26}Mg_{Spl} > \delta^{26}Mg_{Cpx} = \delta^{26}Mg_{Opx} = \delta^{26}Mg_{Ol} > \delta^{26}Mg_{Grt}$ (Table 3, Fig. 4), which is consistent with a previous study (Hu et al. 2016). In addition, clinopyroxene (δ^{26}Mg = −1.54 ± 0.04) and phlogopite separates (δ^{26}Mg = −1.50 ± 0.03) from the phlogopite clinopyroxenite (DMP09-21) have magnesium isotope compositions which are identical to their corresponding whole rock (δ^{26}Mg = −1.53 ± 0.04) within analytical uncertainties.

Discussion

Origin of the Hannuoba pyroxenites

The Hannuoba pyroxenites have been variably interpreted to be the products of modal metasomatism/melt–rock reaction (Song and Frey 1989; Liu et al. 2005), high-pressure cumulates from basaltic magmas (Fan et al. 2001; Xu 2002) or subsolidus differentiates produced by modal segregation of different minerals within the upper mantle (Chen et al. 2001). Based on geochemical features, Xu (2002) and Liu et al. (2005) argued that modal segregation is unlikely for either type of pyroxenites. In this study, both the Cr-diopside pyroxenites and Al-augite pyroxenites show cumulate texture, highly variable Mg#, low Ni and Cr contents, and convex REE abundance patterns with very low abundances of incompatible elements such as Rb, Ba, Th and U (Figs. 1, 2; supplementary Fig. 3). These characteristics are similar to the Al- and Cr-pyroxenites from the Hannuoba reported by Xu (2002), Liu et al. (2005) and Hu et al. (2016), which were ascribed to high-pressure fractional crystallization from parental melt. Based on the REE compositions of clinopyroxenes and the partition coefficients of REE between clinopyroxene and melt (Hart and Dunn 1993; Hauri et al. 1994; Johnson. 1998), parental melt compositions can be estimated. In a primitive mantle normalized diagram (Supplementary Fig. 5), the melts display apparent HFSE depletion, a feature not seen in the host basalts. Therefore, the host basalts can be precluded as the precursor melts of the Cr-diopside pyroxenites and Al-augite pyroxenites. Moreover, the Cr-diopside pyroxenites and Al-augite pyroxenites exhibit extremely variable Sr and Nd isotopic compositions compared to the host basalts (Supplementary Fig. 4). These observations further preclude the cognate origin of the majority of pyroxenites and host basalts. The highly variable REE concentrations of the parental melts of the Hannuoba Cr-diopside pyroxenites and Al-augite pyroxenites suggest that they cannot have been formed through crystallization from a single progressively fractionating mafic liquid (Supplementary Fig. 5). In other words, they likely represent crystallization products of two different precursor melts. The significant difference between the Cr-diopside pyroxenite and

Al-augite pyroxenite Sr–Nd isotopic compositions further supports this conclusion (Supplementary Table 4 and Supplementary Fig. 4). The relatively higher Mg# and slightly higher temperature estimates determined for clinopyroxene from the Cr-diopside pyroxenites (Table 1) suggest that they could have crystallized at greater depth than the Al-augite pyroxenites, possibly within the lithospheric mantle. The majority of the Cr-diopside pyroxenites show Sr–Nd isotopic compositions that overlap the Mantle Array. They are isotopically similar to the Hannuoba peridotites, which are thought to be generated from asthenospheric mantle. This implies that the parental magmas of most Cr-diopside pyroxenites were derived from an asthenospheric mantle source. However, the relatively high $^{87}Sr/^{86}Sr$ and low ε_{Nd}, along with marked HFSE depletion in a few Cr-diopside pyroxenites indicate the involvement of continental crust components in their mantle source.

Most Al-pyroxenites plot below the MORB-OIB-IAB trend on a $^{87}Sr/^{86}Sr$ versus ε_{Nd} plot, falling in the granulite area (Supplementary Fig. 4). They are negatively correlated and are confined to the field of enriched mantle (Supplementary Fig. 4). The ubiquitous HFSE depletion and extremely enriched Sr and Nd isotopic compositions require the involvement of continental crust in their mantle sources. Based on these petrological and geochemical features, Xu (2002) interpreted the the Sm–Nd compostions of the Al-pyroxenites as representing a mixing array and suggested that they were generated by mixing an asthenospheric melt with variable amounts of delaminated lower crustal materials. The relatively low Mg# number and high Al and Fe contents in these Al-augite pyroxenites, coupled with the low Cr content in the clinopyroxene and the geothermobarometric estimations, show that they may have originated as ultramafic cumulates, close to the crust-mantle boundary.

Melts parental to pyroxenites are frequently considered as important agents of mantle metasomatism (Menzies et al. 1985; Bodinier et al. 1990). However, pyroxenites themselves may also be metasomatized (Garrido and Bodinier 1999). The phlogopite clinopyroxene (DMP09-21), which has a high modal phlogopite content, provides clear evidence that the pyroxenites from Hannuoba were modally metasomatized (Fig. 1g, h). Sample DMP09-21 also has the highest K_2O, TiO_2, $A1_2O_3$ contents and highest degree of light-REE enrichment relative to the other samples (Fig. 2, supplementary Fig. 3). The Mg#s of clinopyroxene and phlogopite from this sample are unrelated (Supplementary Table 2), indicating that phlogopite formed later due to the reaction of a fractionated, K, Ba, Ti and REE rich melt with pre-existing clinopyroxene. The clinopyroxenes probably formed originally as cumulate minerals, whereas the phlogopites crystallized during percolation of the melt through the clinopyroxenite.

In contrast to the Hannuoba Cr-diopside pyroxenites and Al-augite pyroxenites, the garnet pyroxenites from Hannuoba have high and uniform Ni contents and Mg# (85–90) (Supplementary Table 1, Supplementary Fig. 2), overlapping the values for the wall rock peridotites. The clinopyroxenes from the garnet pyroxenites are enriched in incompatible elements (e.g., Rb, K, Na, Sr, Ba, Th, U and LREE) (Supplementary Fig. 3). In addition, composite xenoliths consisting of peridotite veined by garnet pyroxenite also occur (Fig. 1i, j). The grain size and orthopyroxene/clinopyroxene mode in these composite xenoliths gradually increase from the peridotite wall into the pyroxenite vein (Fig. 1m, n). Garnet pyroxenite xenoliths from Hannuoba have highly variable Sr isotopic compositions (Supplementary Fig. 4). The majority of garnet pyroxenites exhibit relativly higher $^{87}Sr/^{86}Sr$ values at a given ε_{Nd} than the other two groups of pyroxenite (Supplementary Fig. 4). Based on these petrological and geochemical features, and zircon U–Pb dating of composite xenoliths of garnet pyroxenite + peridotite, Liu et al. (2005, 2010) proposed that the garnet pyroxenites are products of the interaction of the lithospheric peridotites with underplated melts, which resulted in formation of pyroxene at the expense of olivine. In some cases, garnet would also form at sufficiently high pressures and/or water fugacities. The garnet and clinopyroxene-rich features suggest that the underplated melt, rich in Al_2O_3 and CaO, was probably derived from an ancient subducted oceanic slab. This has been confirmed in recent experiments by Wang et al. (2010) and Zhang et al. (2010), which successfully reproduced similar garnet pyroxenites by reacting a Hannuoba spinel peridotite with a quartz eclogite from central China.

Fe and Mg isotopic variations

The results presented in "Iron isotopes" and "Magnesium isotopes" section demonstrate that considerable Fe and Mg isotopic heterogeneity exists at both mineral and bulk rock scales in the mantle pyroxenites from Hannuoba. This feature suggests a genetic link between the pyroxenites and different episodes of melt activity in the Hannuoba lithospheric mantle. In the following sections we first address whether Fe and Mg isotope equilibrium was achieved among minerals in the studied samples and then discuss the origins of the observed variations and their broader implications for the Fe and Mg isotopic geochemistry of the mantle.

Inter-mineral Fe and Mg isotope fractionation

Equilibrium inter-mineral isotope fractionations are theoretically driven by differences in the bonding environment. In general, a lower coordination number (CN) will lead to

stronger bonds favouring the incorporation of heavy isotopes (e.g., Urey 1947; Bigeleisen and Mayer 1947; Schauble 2004). This theoretical prediction has been used to explain inter-mineral stable isotope fractionation in peridotite and pyroxenite xenoliths for Fe and Mg isotopes (Liu et al. 2011; Xiao et al. 2013; Zhao et al. 2015; Macris et al. 2015; Roskosz et al. 2015; Hu et al. 2016). As discussed in Young et al. (2015), the coordination of Fe bonded to O in mantle minerals varies (e.g., CN = 6 for olivine (Ol), orthopyroxene (Opx), clinopyroxene (Cpx) and phlogopite (Phl) but CN = 4 in spinel (Spl) and CN = 8 for garnet (Grt)). In addition, cation substitution has been suggested to exert a secondary control on the Fe isotopic composition of spinel (Young et al. 2015; Macris et al. 2015; Roskosz et al. 2015), as it has both tetrahedral and octahedral sites available for Fe. Macris et al. (2015) and Young et al. (2015) predicted a sequence of enriched δ^{57}Fe in the following order: Spl > Cpx > Opx ≥ Ol > Grt in typical mantle xenoliths based on the ionic model. Among mantle minerals, the Mg coordination number in Ol, Opx, Cpx, Phl and hornblende is the same (CN = 6), but the value is different in Spl (CN = 4) and Grt (CN = 8). Therefore, garnets are enriched in light Mg isotopes while spinels have a greater affinity for heavy Mg isotopes than coexisting silicate minerals (OL, Opx, Cpx, Phl and hornblende) when equilibrium Mg exchange is achieved (Liu et al. 2011, Schauble 2011; Huang et al. 2013; Wu et al. 2015). A theoretical relative ordering of ^{26}Mg/^{24}Mg enrichment is Spl > Cpx ≥ Opx ≥ Ol > Grt, which has been confirmed by the analysis of natural samples (Li et al. 2011, 2016b; Liu et al. 2011; Wang et al. 2012, 2014a, 2014b, 2015a, 2015b; Xiao et al. 2013). Below, we examine the nature of inter-mineral Fe and Mg isotope fractionations in Hannuoba pyroxenites in detail by comparing our mineral data with that derived in theoretical studies (Young et al. 2009, 2015; Schauble 2011; Huang et al. 2013; Wu et al. 2015; Macris et al. 2015; Roskosz et al. 2015; Li et al. 2016b).

The inter-mineral Fe fractionation ($\Delta^{57}Fe_{X-Y} = \delta^{57}Fe_X - \delta^{57}Fe_Y$, where X and Y refer to the different minerals) varies from −0.03 to 0.02‰, with an average of −0.01 ± 0.06‰ (2SD, n = 2), between Opx and Ol: from −0.00 to 0.13‰, with an average of 0.03 ± 0.13‰ (2SD, n = 3) between Cpx and Ol and from 0.04 to 0.08‰, with an average of 0.06 ± 0.05‰ (2SD, n = 8) between Cpx and Opx in Hannuoba Cr-diopside pyroxenites and Al-augite pyroxenites. These inter-mineral fractionation values all fall very close to, or on the equilibrium fractionation lines of, olivine-pyroxenes at mantle temperatures (800 ~ 1000 °C, Macris et al. 2015) (Fig. 5a–c), suggesting possible Fe isotopic equilibrium fractionation between olivine and pyroxenes in the Hannuoba Cr-diopside pyroxenites and Al-augite pyroxenites. The following Δ^{57}Fe values have been determined: $\Delta^{57}Fe_{Spl-Ol}$ varies from 0.15 to 0.18‰, with an average of 0.16 ± 0.04‰ (2SD, n = 2); $\Delta^{57}Fe_{Spl-Opx}$ varies from 0.15 to 0.18‰, with an average of 0.17 ± 0.04‰ (2SD, n = 2); $\Delta^{57}Fe_{Spl-Cpx}$ varies from 0.13 to 0.15‰, with an average of 0.14 ± 0.04‰ (2SD, n = 2). These values also fall very close to or on the equilibrium fractionation lines of spinel-silicate minerals at mantle temperature (800 ~ 1000 °C, Macris et al. 2015) (Fig. 5d–f), which suggests an equilibrium Fe isotope fractionation between spinel and these silicate minerals in the Hannuoba Cr-diopside pyroxenites and Al-augite pyroxenites. Over all, the constituent minerals from the Cr-diopside pyroxenites and Al-augite pyroxenites have ^{57}Fe/^{54}Fe that fall in the following order: $\delta^{57}Fe_{Spl} > \delta^{57}Fe_{Cpx} > \delta^{57}Fe_{Opx} \geq \delta^{57}Fe_{Ol}$ (Table 2, Fig. 3). This is consistent with expectations based on the coordination and valence state of iron as described in the ionic model (Macris et al. 2015). Thus, Fe isotopes are likely in equilibrium among most olivine, clinopyroxene, orthopyroxene and spinel, at hand-sample scale, for the Hannuoba Cr-diopside pyroxenites and Al-augite pyroxenites.

Phlogopite from the phlogopite clinopyroxenite has a Fe isotopic composition similar to the clinopyroxene suggesting that phlogopite-clinopyroxene Fe isotope fractionation is in equilibrium. This is also in agreement with predictions from theoretical considerations based on Fe–O bonding strengths (Fe bonded to O in clinopyroxene and phlogopite is the same, e.g., CN = 6). However, elemental compositions and mineralogy suggest that phlogopite was produced by later metasomatic processes as it is not in chemical equilibrium with clinopyroxene. Therefore, kinetic fractionation associated with mantle metasomatism cannot be ruled out.

Compared to the Cr-diopside pyroxenites and Al-augite pyroxenites, large degrees of Fe isotope fractionation ($\Delta^{57}Fe_{Opx-Ol}$ = −0.01 to 0.37‰; $\Delta^{57}Fe_{Cpx-Ol}$ = 0.11 to 0.42 ‰ and $\Delta^{57}Fe_{Spl-Ol}$ = 0.16 to 0.58‰) occur between the olivine and other minerals in the Hannuoba garnet-bearing pyroxenites. These observed data stand in marked contrast to the calculated equilibrium Fe isotope fractionation between olivine and other minerals at mantle temperatures (800 ~ 1000 °C, Macris et al. 2015), (Fig. 5), indicating disequilibrium isotope fractionation. Large Fe isotope fractionation ($\Delta^{57}Fe_{Sp-Ol}$ = 0.16 to 0.58‰; $\Delta^{57}Fe_{Sp-Opx}$ = −0.05 to 0.39‰; $\Delta^{57}Fe_{Sp-Cpx}$ = 0.05–0.14‰) also occurs between the spinel and silicate minerals (olivine and pyroxenes) in the Hannuoba garnet-bearing pyroxenites. The measured inter-mineral fractionation in most Hannuoba garnet-bearing pyroxenites falls outside the theoretical calculation of Fe isotope fractionation between spinel and silicate minerals (800 ~ 1000 °C, Macris et al. 2015), (Fig. 5c, e, f), suggesting that the spinel and silicate minerals in most garnet-bearing pyroxenites have not reached Fe isotopic equilibrium. Compared to the sixfold

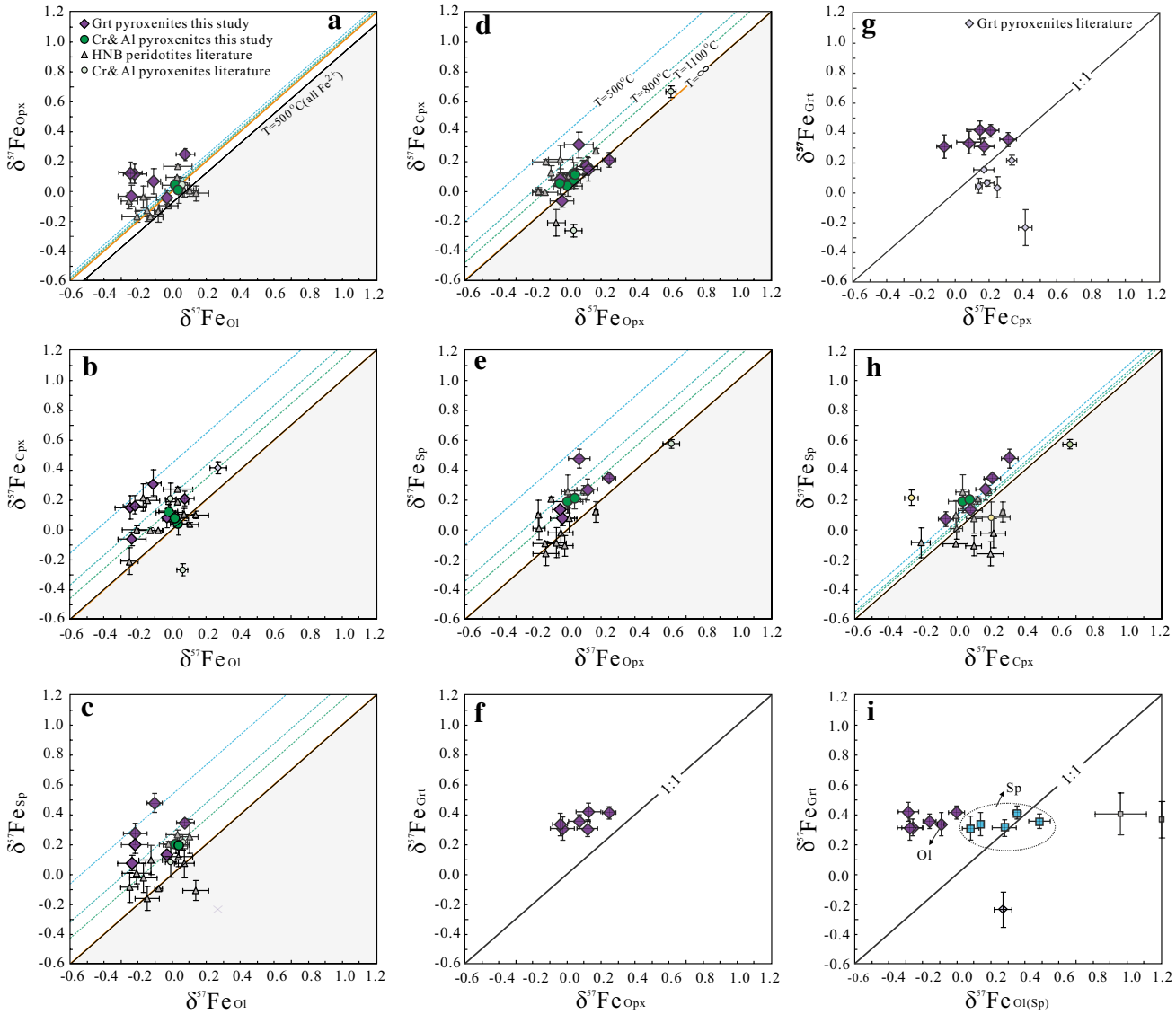

Fig. 5 Fe isotope fractionation between minerals in Hannuoba pyroxenite xenoliths. The calculated equilibrium Fe isotope fractionation lines are from Macris et al. (2015). Data are from Table 2. *Error bars* are 2 SD

coordinated Fe in olivine and pyroxene, Fe is eightfold coordinated in garnet and fourfold coordinated in spinel. Therefore, all else being equal, olivine, pyroxene and spinel should have higher $^{57}Fe/^{54}Fe$ ratios than garnet at equilibrium, by virtue of shorter Fe–O bond lengths (Young et al. 2015). However, all garnets analysed in this work have significantly heavier Fe isotopic compositions relative to coexisting Ol, pyroxenes and spinels (Table 2): $\Delta^{57}Fe_{Grt\text{-}Ol}$ varies from 0.34 to 0.66‰; $\Delta^{57}Fe_{Grt\text{-}Opx}$ varies from 0.17 to 0.37‰; $\Delta^{57}Fe_{Grt\text{-}Cpx}$ varies from 0.04 to 0.37‰; $\Delta^{57}Fe_{Grt\text{-}Spl}$ varies from −0.02 to 0.47‰. The $^{57}Fe/^{54}Fe$ for constituent minerals from the garnet-bearing pyroxenites is ordered as follows: $\delta^{57}Fe_{Grt} > \delta^{57}Fe_{Spl} > \delta^{57}Fe_{Cpx} > \delta^{57}Fe_{Opx} > \delta^{57}Fe_{Ol}$ (Table 2, Fig. 3). This is inconsistent with theoretical calculation (Young et al. 2015), indicating disequilibrium isotope fractionation. Petrological and geochemical studies further support disequilibrium processes, as shown by the classic spinel-cored garnets in these samples (Fig. 1i, j), indicating late-stage mineral reactions. Therefore, the isotope disequilibria between mantle minerals in these garnet-bearing pyroxenites may result from late-stage processes that affected the isotopic compositions of minerals in the garnet-bearing pyroxenites.

Mg isotope fractionation ($\Delta^{26}Mg_{X-Y} = \delta^{26}Mg_X - \delta^{26}Mg_Y$, where X and Y refer to the different minerals) between most coexisting pyroxene and olivine in this study is barely analytically resolvable, with $\Delta^{26}Mg_{Cpx\text{-}Ol} = 0.01$–$0.03‰$ ($n = 2$), $\Delta^{26}Mg_{Opx\text{-}Ol} = 0.03‰$ ($n = 1$) and

$\Delta^{26}Mg_{Cpx\text{-}Opx}$ = 0.01 to 0.06‰ (n = 3). This is consistent with previous observations made on pyroxenites (Hu et al. 2016) and is also broadly consistent with theoretical predictions for inter-mineral equilibrium fractionation at high temperature (Young et al. 2009; Schauble 2011; Huang et al. 2013). This suggests that Mg isotopes are in equilibrium between pyroxene and olivine at the hand sample scale. However, large Mg isotope fractionations ($\Delta^{26}Mg_{Cpx\text{-}Grt}$ = 0.35‰; $\Delta^{26}Mg_{Opx\text{-}Grt}$ = 0.34‰; $\Delta^{26}Mg_{Ol\text{-}Grt}$ = 0.34‰) occur between garnet and other silicate minerals in the garnet-bearing pyroxenite (Table 3, Fig. 6a, b). This is consistent with previously published inter-mineral Mg isotope variations between garnet and other silicate minerals from the Hannuoba garnet-bearing pyroxenite (Hu et al. 2016). However, these observations stand in marked contrast to the theoretical predictions of equilibrium inter-mineral fractionation factors at mantle temperatures (e.g., $\Delta^{26}Mg_{Cpx\text{-}Grt}$ = 0.60‰; $\Delta^{26}Mg_{Opx\text{-}Grt}$ = 0.59‰ and $\Delta^{26}Mg_{Ol\text{-}Grt}$ = 0.50‰ at 1000 °C, Huang et al. 2013; Li et al. 2016b), (Fig. 6a, b), indicating disequilibrium isotope fractionation. Therefore, we conclude that these garnets had not yet reached isotopic equilibrium with the co-existing olivine and pyroxene, consistent with previous work (Hu et al. 2016). Large Mg isotope fractionations ($\Delta^{26}Mg_{Sp\text{-}Ol}$ = 0.39‰; $\Delta^{26}Mg_{Sp\text{-}Opx}$ = 0.39‰; $\Delta^{26}Mg_{Sp\text{-}Cpx}$ = 0.38‰; $\Delta^{26}Mg_{Sp\text{-}Grt}$ = 0.72‰) also occur between the spinel and silicate minerals (olivine, pyroxenes and garnet) in the garnet pyroxenite. The inter-mineral fractionation in this garnet pyroxenite fall outside the theoretical calculation of the Mg isotope fractionation between spinel and silicate minerals (0.5–0.6‰, 1000 °C, Schauble 2011), suggesting that the spinel and silicate minerals in the garnet pyroxenite had not reached Mg isotopic equilibrium. Clinopyroxene and phlogopite from the phlogopite clinopyroxenite (DMP09-21) have similar Mg isotopic compositions (Table 3, Fig. 4), consistent with the implications suggested from Fe isotope analysis. However, as mentioned above, phlogopite in this sample appears to be a secondary product of metasomatism. Therefore, kinetic fractionation associated with mantle metasomatism cannot be fully excluded.

Homogeneity of Fe and Mg isotopes in Cr-diopside pyroxenites and Al-augite pyroxenites

Both the Cr-diopside pyroxenites and Al-augite pyroxenites from Hannuoba analysed here show a limited variation in $\delta^{57}Fe$ (−0.01 to 0.09) even though they are chemically diverse. This value overlaps the range of spinel peridotites from Hannuoba (Table 2, Fig. 2). The average $\delta^{57}Fe$ of the Cr-diopside pyroxenites and Al-augite pyroxenites studied is 0.03 ± 0.08 (2SD, n = 6) (Table 2). This value overlaps (within uncertainty) the fertile upper-mantle value ($\delta^{57}Fe$ = 0.09 ± 0.04, Zhao et al. 2015) inferred from peridotites without evidence of previous melt depletion and metasomatism from Yangyuan, NCC and the mean mafic Earth reference value ($\delta^{57}Fe$ = 0.10 ± 0.03, Poitrasson et al. 2013). The narrow $\delta^{57}Fe$ range yielded by the whole rocks and the equilibrium inter-mineral Fe isotope fractionations between the co-existent mineral phases in the Cr-diopside pyroxenites and Al-augite pyroxenites are consistent with the implications of Mg isotope signatures for

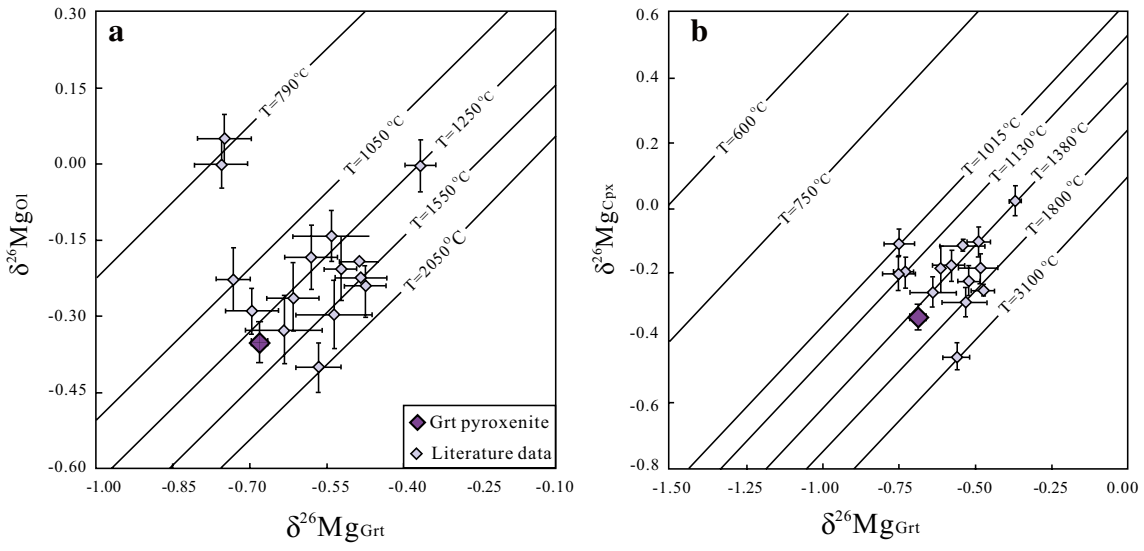

Fig. 6 Correlation of $\delta^{26}Mg_{Grt}$ vs. $\delta^{26}Mg_{Cpx}$ and $\delta^{26}Mg_{Ol}$ at different equilibrium temperatures. The calculated equilibrium Mg isotope *fractionation lines* are from Huang et al. (2013) by assuming the equilibrium pressure of 1.5 GPa throughout. Data are from Table 3. *Error bars* are 2 SD

Hannuoba Cr-diopside pyroxenites and Al-augite pyroxenites (Hu et al. 2016).

Our new Mg isotopes data confirm the findings of a previous study, that most Cr-diopside pyroxenites and Al-augite pyroxenites from Hannuoba have homogenous mantle-like Mg isotopic composition, with equilibrated clinopyroxene-orthopyroxene pairs (Fig. 4). These Cr-diopside pyroxenites and Al-augite pyroxenites are interpreted as crystallization products of high-pressure basaltic melts passing through the lithospheric mantle, as discussed in "Origin of Hannuoba pyroxenites" section. There is no correlation between δ^{57}Fe and δ^{26}Mg in Cr-diopside pyroxenites and Al-augite pyroxenites (Fig. 7). No clear co-variations between the whole-rock or mineral Fe isotope compositions of the peridotites from the Cr-diopside pyroxenites and Al-augite pyroxenites and the petrologic or geochemical parameters (e.g., Al_2O_3 and FeO in whole rocks or minerals and Cr#s in clinopyroxene or spinel) could be observed (Fig. 8). All of these features suggest that high-pressure, cumulate-forming processes investigated here do not cause significant Fe and Mg isotopic fractionation in the Hannuoba Cr-diopside pyroxenites and Al-augite pyroxenites and that the Hannuoba Cr-diopside pyroxenites and Al-augite have homogenous Fe and Mg isotopic compositions.

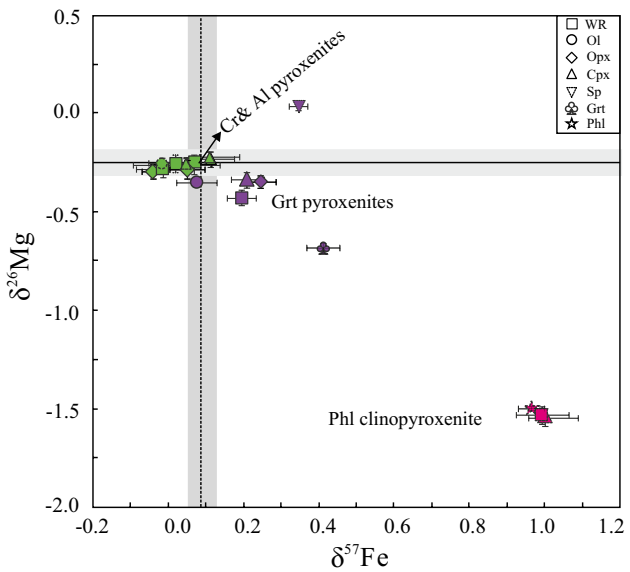

Fig. 7 Fe and Mg isotopic compositions of the Hannuoba pyroxenite xenoliths and minerals. δ^{57}Fe data are from Table 2. δ^{26}Mg data are from Table 3. *Error bars* are 2 SD. The horizontal grey band represents the Mg isotopic composition of the mantle based on studies of global oceanic basalts and peridotites (δ^{26}Mg = −0.25 ± 0.07, 2 SD; Teng et al. 2010). The *solid vertical line* and grand band at δ^{57}Fe = 0.09 ± 0.04‰ is the fertile upper-mantle value, inferred from two spinel peridotites without metasomatism from Yangyuan, NCC (Zhao et al. 2015)

A metasomatic origin for Fe–Mg isotopic variations in garnet-bearing pyroxenites and phlogopite clinopyroxenite

Seven garnet-bearing pyroxenites and their constituent minerals have variable and heavy Fe isotopic values (Table 2, Fig. 3). Most of them display significant inter-mineral isotopic variations, well beyond that expected from equilibrium isotope fractionation at high temperatures (Fig. 5), indicating disequilibrium Fe isotope fractionation. Petrological and geochemical studies have shown that the Hannuoba garnet-bearing pyroxenites were produced by interaction of peridotites with ancient subducted oceanic slab, which resulted in the formation of pyroxene and garnet at the expense of olivine (Liu et al. 2005, 2010). In particular, these garnet-bearing pyroxenites and minerals show increasing δ^{57}Fe with increasing Al_2O_3 and FeO contents (Fig. 8). They also display the strongest deviation toward heavier Fe isotope ratios associated with the lower Cr# in clinopyroxene and spinel (Fig. 8). All of these lines of evidence suggest that the variable and heavy Fe isotopic composition in the bulk rocks and the disequilibrium inter-mineral Fe isotope fractionation in the Hannuoba garnet-bearing pyroxenites were produced through melt-rock interaction. Similar incomplete isotopic exchange processes during melt–rock interaction have been invoked for the inter-mineral Mg isotope disequilibrium found in garnet-bearing pyroxenites from Hannuoba (Hu et al. 2016). Our new data on the garnet pyroxenite from Hannuoba yield a δ^{26}Mg value of −0.43, falling with the range observed for the Hannuoba garnet-bearing pyroxenites (−0.48 to −0.10, Hu et al. 2016). The constituent minerals from this garnet-bearing pyroxenite yield ^{26}Mg/^{24}Mg values that can be ordered as follows: $\delta^{26}Mg_{Spl} > \delta^{26}Mg_{Cpx} = \delta^{26}Mg_{Opx} = \delta^{26}Mg_{Ol} > \delta^{26}Mg_{Grt}$. This is similar to the recent observation by Hu et al. (2016) that garnet minerals have a lighter Mg isotopic composition than co-existing olivine, clinopyroxene, orthopyroxene and spinel. Notably, the order of ^{57}Fe/^{54}Fe for constituent minerals from the Hannuoba garnet-bearing pyroxenites is $\delta^{57}Fe_{Grt} > \delta^{57}Fe_{Spl} > \delta^{57}Fe_{Cpx} > \delta^{57}Fe_{Opx} > \delta^{57}Fe_{Ol}$ as mentioned above. Taken together, these findings imply that the Hannuoba garnet-bearing pyroxenites and the garnets therein have much heavier Fe but lighter Mg isotopic compositions than the expected values assuming equilibrium (Young et al. 2015). Overall there appears to be a negative co-variation between δ^{57}Fe and δ^{26}Mg in Hannuoba garnet pyroxenites, including in the mineral separates (Fig. 7). Several studies have shown that negatively coupled Mg–Fe isotopic compositions are associated with chemical diffusion as these elements inter-diffuse, and the light isotopes of one element always diffuse faster than their heavier counterparts (Dauphas et al. 2010; Teng et al. 2011; Sio et al. 2013). Likewise, we infer

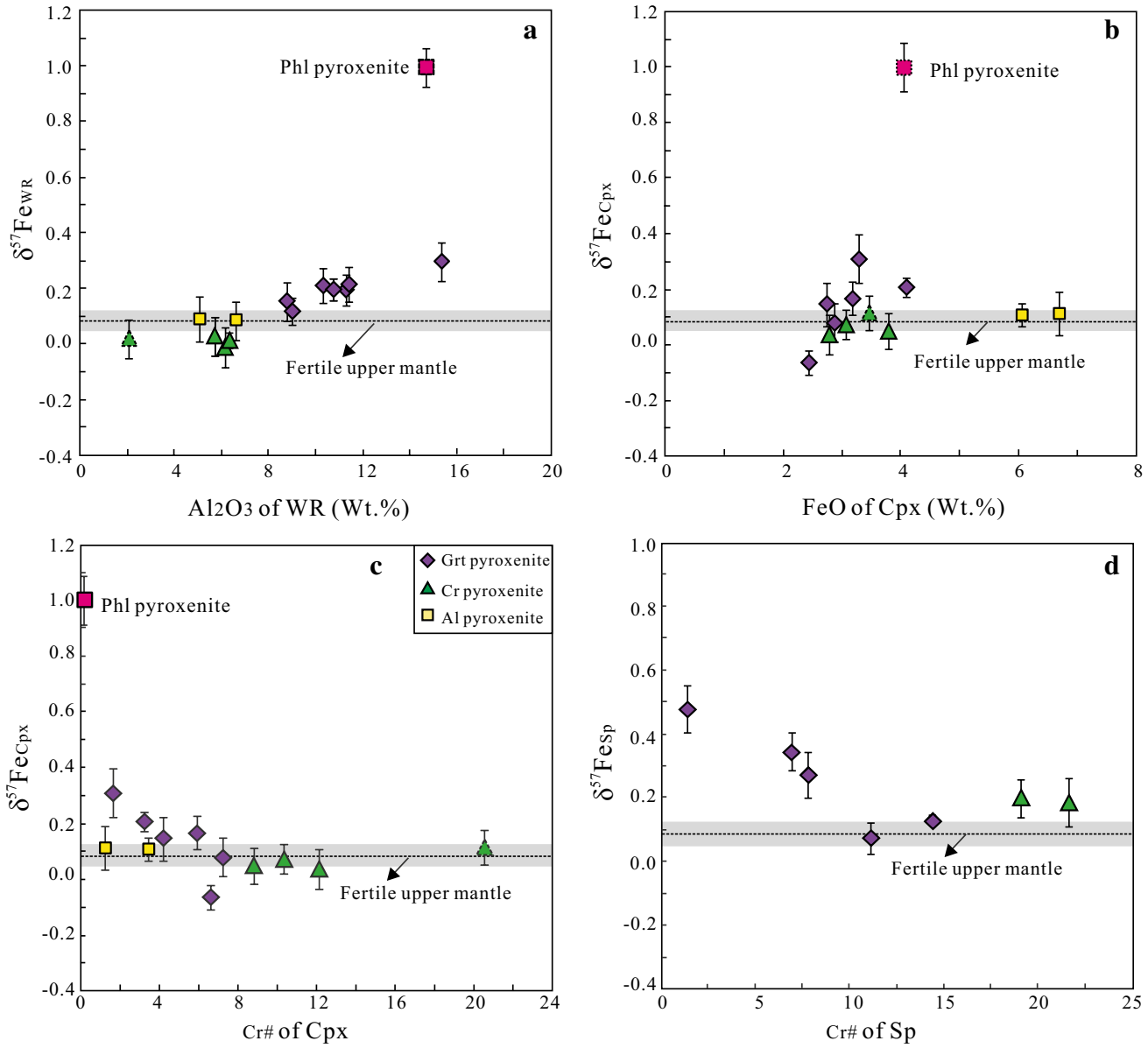

Fig. 8 **a** δ^{57}Fe values of Hannuoba pyroxenite xenoliths against their Al_2O_3 content, **b** δ^{57}Fe values of clinopyroxenes in Hannuoba pyroxenite xenoliths against their FeO content. δ^{57}Fe values of clinopyroxenes (**c**) and spinels (**d**) against their Cr#. The horizontal dash line and grey band at $\delta^{57}Fe = 0.09 \pm 0.04$ is the fertile upper-mantle value inferred from peridotites without evidence of previous melt depletion and metasomatism from Yangyuan, NCC (Zhao et al. 2015). Data are from Table 2, supplementary Tables 1 and 2. *Error bars* are 2 SD

that diffusive processed have resulted in the large Fe and Mg isotopic variations in bulk rocks and disequilibrium inter-mineral Fe and Mg isotope fractionations in the Hannuoba garnet pyroxenites. As mentioned above, the Hannuoba garnet-bearing pyroxenites were products of interaction between multiple silicic melts and peridotite, which resulted in the conversion of olivine to pyroxene and garnet, generating garnet pyroxenites (Liu et al. 2005). In this case, Fe and Mg will be exchanged in mantle minerals during incomplete melt-rock interactions that produced these garnets. As mentioned above, the light isotopes of one element always diffuse faster than the heavier isotopes (Richter et al. 2008, 2009), so Mg–Fe inter-diffusion process will result in a negative co-variation between Fe and Mg isotopic composition.

The phlogopite clinopyroxenite (DMP09-21) analysed here yielded consistent heavy δ^{57}Fe values for the whole rock, clinopyroxene and phlogopite fragments, which are also the heaviest values reported for mantle rocks to date. In particular, the phlogopite clinopyroxenite also has

the lightest δ^{26}Mg (−1.50) values for clinopyroxene and phlogopite fragments and displays the strongest deviation towards a heavier Fe isotope ratio, associated with extremely higher Al_2O_3, FeO but much lower Cr# in the clinopyroxene (Fig. 8). The extremely heavy Fe and light Mg isotopic compositions of the phlogopite clinopyroxenite are likely generated by kinetic effects due to Fe–Mg inter-diffusion during percolation of the melt through the clinopyroxenite.

Implications for a heterogeneous Fe and Mg isotopic composition in the lithospheric mantle

Pyroxenites, a minor but important type of xenolith entrained in both kimberlites and basalts worldwide, are generally regarded as a physical manifestation of mantle heterogeneity. Here, we have shown that considerable Fe isotopic heterogeneity exists at both the mineral and bulk-rock scales in the strongly metasomatized garnet pyroxenites and phlogopite clinopyroxenite from Hannuoba (Fig. 3, Fig. 5). Previous analyses of most oceanic basalts and mantle peridotites yielded consistent δ^{26}Mg values (−0.25 ± 0.07) within the uncertainty of current analytical methods and hence suggest a homogeneous mantle (Handler et al. 2009; Yang et al. 2009; Bourdon et al. 2010; Teng et al. 2010; Huang et al. 2011; Liu et al. 2011; Lai et al. 2015). However, more recent studies on strongly metasomatized peridotites, particularly wehrlites, found that δ^{26}Mg values deviated from the nominal mantle range (Yang et al. 2009; Pogge von Strandmann et al. 2011; Xiao et al. 2013), indicating that the mantle is not completely homogeneous in terms of Mg isotopes. Our new Mg isotopic data on garnet pyroxenites and phlogopite clinopyroxenites, together with previously published data on garnet pyroxenites from the Hannuoba area (Hu et al. 2016), also demonstrate large variations in bulk-rock δ^{26} Mg with evidence for disequilibrium inter-mineral fractionation (Figs. 4, 6). Although garnet pyroxenite and phlogopite clinopyroxenite make up a relatively small volume of mantle constituents, the substantial variations in δ^{57}Fe and δ^{26}Mg observed implies Fe and Mg isotope heterogeneity in the lithospheric mantle resulting from mantle metasomatism, at least locally.

Conclusions

This study presents the first high-precision, combined Fe and Mg isotopic data for mantle pyroxenites, coupled with whole rock and mineral chemical compositions. The following conclusions can be drawn:

1. Both Cr-diopside pyroxenites and Al-augite pyroxenites display limited Fe and Mg isotopic variations with δ^{57}Fe ranging from −0.01 to 0.09 and δ^{26}Mg ranging from −0.28 to −0.25, respectively. These values are indistinguishable from the normal upper mantle, indicating that there is no significant Fe–Mg isotopic fractionation during the high-pressure, cumulate-forming processes investigated here.
2. The garnet-bearing pyroxenites have heterogeneous Fe and Mg isotopic compositions, consistent with their origin as reaction products between mantle peridotites and melts from a subducted oceanic slab. The large and negatively correlated Mg and Fe isotopic compositions in the Hannuoba garnet-bearing pyroxenites most likely reflect kinetic isotopic fractionation during melt-peridotite reaction.
3. The phlogopite clinopyroxenite and mineral separates from Hannuoba show extremely heavy δ^{57}Fe (0.99) and light δ^{26}Mg (−1.50). Such a negative correlation between Fe and Mg isotopic compositions in phlogopite clinopyroxenite and mineral separates is strongly linked to kinetic isotope fractionation due to Fe–Mg inter-diffusion, occurring during when the reacting melt percolates through the rock.

Acknowledgements We thank Zhuying Chu for Rb–Sr and Sm–Nd isotope analyses at the Institute of Geology and Geophysics (IGG), Chinese Academy of Sciences and Huimin Yu for Fe and Mg isotopes analyses at the Chinese Academy of Sciences Key Laboratory of Crust-Mantle Materials and Environments, University of Science and Technology of China (USTC). Jifeng Ying is thanked for the helpful discussion. This work was financially supported by the National Science Foundation of China (41373041 and 41673021 to Xin Miao Zhao). Associate editor Franck Poitrasson, Michel Grégoire and one anonymous reviewer are thanked for their thoughtful and constructive reviews which substantially improved the paper.

References

Ackerman L, Jelinek E, Medaris LG, Jezek J, Siebel W, Strnad L (2009) Geochemistry of Fe-rich peridotites and associated pyroxenites from Horní Bory, Bohemian Massif: insights into subduction-related melt-rock reactions. Chem Geol 259:152–167

An YJ, Wu F, Xiang YX, Nan XY, Yu X, Yang JH, Yu HM, Xie LW, Huang F (2014) High-precision Mg isotope analyses of low-Mg rocks by MC-ICP-MS. Chem Geol 390:9–21

An Y, Huang JX, Griffin WL, Liu C, Huang F (2017) Isotopic composition of Mg and Fe in garnet peridotites from the Kaapvaal and Siberian Cratons. Geochim Cosmochim Acta 200(1):167–185

Basu AR, Wang JW, Huang WK, Xie GH, Tatsumoto M (1991) Major element, REE, and Pb, Nd and Sr isotopic geochemistry of Cenozoic volcanic rocks of eastern China: implications for their origin from suboceanic-type mantle reservoirs. Earth Planet Sci Lett 105:149–169

Beard BL, Johnson CM (2004) Inter-mineral Fe isotope variations in mantle-derived rocks and implications for the Fe geochemical cycle. Geochim Cosmochim Acta 68(22):4727–4743

Beyer EE, Griffin WL, O'Reilly SY (2006) Transformation of archaean lithospheric mantle by refertilization: evidence from exposed peridotites in the Western Gneiss Region. Norway J Petrol 47:1611–1636

Bigeleisen J, Mayer MG (1947) Calculation of equilibrium constants for isotopic exchange reactions. J Chem Phys 15:261–267

Bizzarro M, Paton C, Larsen K, Schiller M, Trinquier A, Ulfbeck D (2011) High-precision Mg-isotope measurements of terrestrial and extraterrestrial material by HR-MC-ICPMS-implications for the relative and absolute Mg-isotope composition of the bulk silicate Earth. J Anal Atom Spectrom 26(3):565–577

Bodinier JL, Godard M (2014) Orogenic, ophiolitic, and abyssal peridotites. In: Carlson RW (ed) The mantle and core. Treatise on geochemistry. Elsevier-Pergamon, Oxford

Bodinier JL, Vaseur G, Vernieres J, Dupuy C, Fabries J (1990) Mechanisms of mantle metasomatism: geochemical evidence from the Lherz orogenic peridotite. J Petrol 31:597–628

Bourdon B, Tipper ET, Fitoussi C, Stracke A (2010) Chondritic Mg isotope composition of the Earth. Geochim Cosmochim Acta 74(17):5069–5083

Brey GP, Köhler T (1990) Geothermobarometry in four-phase lherzolites II: new thermobarometers, and practical assessment of existing thermobarometers. J Petrol 31(6):1353–1378

Chen SH, O'Reilly SY, Zhou XH, Griffin WL, Zhang GH, Sun M, Feng JL, Zhang M (2001) Thermal and petrological structure of the lithosphere beneath Hannuoba, Sino-Korean Craton, China: evidence from xenoliths. Lithos 56(4):267–301

Choi SH, Mukasa SB, Zhou XH, Xian XH, Andronikov AV (2008) Mantle dynamics beneath East Asia constrained by Sr, Nd, Pb and Hf isotopic systematics of ultramafic xenoliths and their host basalts from Hannuoba, North China. Chem Geol 248:40–61

Chu ZY, Wu FY, Walker RJ, Rudnick RL, Pitcher L, Puchtel IS, Yang YH, Wilde SA (2009) Temporal evolution of the lithospheric mantle beneath the Eastern North China Craton. J Petrol 50:1857–1898

Craddock PR, Dauphas N (2011) Iron isotopic compositions of geological reference materials and chondrites. Geostand Geoanal Res 35(1):101–123

Dantas C, Grégoire M, Koester E, Conceição RV, Rieck N (2009) The lherzolite–websterite xenolith suite from Northern Patagonia (Argentina): evidence of mantle–melt reaction processes. Lithos 107(1):107–120

Dauphas N, Craddock PR, Asimow PD, Bennett VC, Nutman AP, Ohnenstetter D (2009) Iron isotopes may reveal the redox conditions of mantle melting from Archean to Present. Earth Planet Sci Lett 288(1–2):255–267

Dauphas N, Teng FZ, Arndt NT (2010) Magnesium and iron isotopes in 2.7 Ga Alexo komatiites: mantle signatures, no evidence for Soret diffusion, and identification of diffusive transport in zoned olivine. Geochim Cosmochim Acta 74(11):3274–3291

Dauphas N, Roskosz M, Alp EE, Neuville DR, Hu MY, Sio CK, Tissot FLH, Zhao J, Tissandier L, Cordier C (2014) Magma redox and structural controls on iron isotope variations in Earth's mantle and crust. Earth Planet Sci Lett 398:127–140

Downes H (2001) Formation and modification of the shallow subcontinental lithospheric mantle: a review of geochemical evidence from ultramafic xenolith suites and tectonically emplaced ultramafic massifs of western and central Europe. J Petrol 42:233–250

Downes H (2007) Origin and significance of spinel and garnet pyroxenites in theshallow lithospheric mantle: ultramafic massifs in orogenic belts in Western Europe and NW Africa. Lithos 99:1–24

Fan QC, Hooper PR (1991) The Cenozoic basaltic rocks of eastern China: petrology and chemical composition. J Petrol 32:765–810

Fan WM, Zhang HF, Baker J, Jarvis KE, Mason PRD, Menzies MA (2000) On and off the North China Craton: where is the Archaean keel? J Petrol 41(7):933–950

Fan QC, Sui JL, Liu RX, Zhou XM (2001) Eclogite facies garnet-pyroxenite xenoliths in Hannuoba area: new evidence of magma underplating (in Chinese with English Abs.). Acta Pet. Sin 17:1–6

Fan QC, Zhang HF, Sui JL, Zhai MG, Sun Q, Li N (2005) Magma underplating and Hannuoba present crust-mantle transitional zone composition: xenolith petrological and geochemical evidence. Sci China Ser D 48:1089–1105 **(in Chinese with English abstract)**

Galy A, Yoffe O, Janney PE, Williams RW, Cloquet C, Alard O, Halicz L, Wadhwa M, Hutcheon ID, Ramon E, Carignan J (2003) Magnesium isotope heterogeneity of the isotopic standard SRM 980 and new reference materials for magnesium isotope ratio measurements. J Anal At Spectrom 18:1352–1356

Gao S, Rudnick RL, Carlson RW, McDonough WF, Liu Y (2002) Re − Os evidence for replacement of ancient mantle lithosphere beneath the North China Craton. Earth Planet Sci Lett 198:307–322

Gao S, Rudnick RL, Yuan HL, Liu XM, Liu YS, Xu WL, Ling WL, Ayers J, Wang XC, Wang QH (2004) Recycling lower continental crust in the North China craton. Nature 432:892–897

Garrido CJ, Bodinier JL (1999) Diversity of mafic rocks in the Ronda peridotite: evidence for pervasive melt-rock reaction during heating of subcontinental lithosphere by upwelling asthenosphere. J Petrol 40:729–754

Griffin WL, O'Reilly SY, Ryan CG (1992) Composition and thermal structure of the lithosphere beneath South Africa, Siberia and China: proton microprobe studies. In Proceedings of the International Symposium on Cenozoic Volcanic rocks and deep-seated xenoliths of China and its Environs, Beijing pp 65–66

Griffin WL, Zhang AD, O'Reilly SY, Ryan CG (1998) Phanerozoic evolution of the lithosphere beneath the Sino-Korean Craton. In: Flower MFJ, Chung SL, Lo CH, Lee TY (eds) Mantle dynamics and plate interactions in East Asia. American Geophysical Union, Washington, pp 107–126

Handler MR, Baker JA, Schiller M, Bennett VC, Yaxley GM (2009) Magnesium stable isotope composition of Earth's upper mantle. Earth Planet Sci Lett 282(1):306–313

Hart SR, Dunn T (1993) Experimental CPX/melt partitioning of 24 trace elements. Contrib Mineral Petrol 113(1):1–8

Hauri EH, Wagner TP, Grove TL (1994) Experimental and natural partitioning of Th, U, Pb and other trace elements between garnet, clinopyroxene and basaltic melts. Chem Geol 117:149–166

Hibbert KEJ, Williams HM, Kerr AC, Puchtel IS (2012) Iron isotopes in ancient and modern komatiites: evidence in support of an oxidised mantle from Archean to present. Earth Planet Sci Lett 321:198–207

Hirschmann MM, Stolper EM (1996) A possible role for garnet pyroxenite in the origin of the "garnet signature" in MORB. Contrib Mineral Petrol 124:185–208

Hu Y, Teng FZ, Zhang HF, Xiao Y, Su BX (2016) Metasomatism-induced mantle magnesium isotopic heterogeneity: evidence from pyroxenites. Geochim Cosmochim Acta 185:88–111

Huang F, Zhang ZF, Lundstrom CC, Zhi XC (2011) Iron and magnesium isotopic compositions of peridotite xenoliths from Eastern China. Geochim Cosmochim Acta 75(12):3318–3334

Huang F, Chen LJ, Wu ZQ, Wang W (2013) First-principles calculations of equilibrium Mg isotope fractionations between garnet, clinopyroxene, orthopyroxene, and olivine: implications for Mg isotope thermometry. Earth Planet Sci Lett 367:61–70

Jacob D (2004) Nature and origin of eclogite xenoliths from kimberlites. Lithos 77:295–316

Johnson KTM (1998) Experimental determination of partition coefficients for rare earth and high-field-strength elements between clinopyroxene, garnet, and basalticmelt at high pressures. Contrib Mineral Petrol 133:60–68

Keshav S, Sen G, Presnall DC (2007) Garnet-bearing xenoliths from Salt Lake Crater, Oahu, Hawaii: high-pressure fractional crystallization in the oceanic mantle. J Petrol 48:1681–1724

Konter JG, Pietruszka AJ, Hanan BB, Finlayson VA, Craddock PR, Jackson MG, Dauphas N (2016) Unusual δ^{56} Fe values in Samoan rejuvenated lavas generated in the mantle. Earth Planet Sci Lett 450:221–232

Korenaga J, Kelemen PB (2000) Major element heterogeneity in the mantle source of the North Atlantic igneous province. Earth Planet Sci Lett 184:251–268

Lai YJ, Strandmann PAE, Dohmen R, Takazawa E, Tim Elliott (2015) The influence of melt infiltration on the Li and Mg isotopic composition of the Horoman Peridotite Massif. Geochim Cosmochim Acta 164(1):318–332

Lee CT, Rudnick RL (1999) Compositionally stratified cratonic lithosphere: petrology and geochemistry of peridotite xenoliths from the Labait volcano, Tanzania. In: Gurney JJ, Gurney JL, Pascoe MD (eds) Proceedings of the 7th International Kimberlite Conference l. Red Roof Design, Cape Town, pp 503–521

LeRoux V, Bodinier JL, Tommasi A, Alard O, Dautria JM, Vauchez A, Riches AJV (2007) The Lherz spinel lherzolite: refertilized rather than pristine mantle. Earth Planet Sci Lett 259:599–612

LeRoux V, Bodinier JL, Alard O, O'Reilly SY, Griffin WL (2009) Isotopic decoupling during porous melt flow: a case-study in the Lherz peridotite. Earth Planet Sci Lett 279:76–85

Li WY, Teng FZ, Xiao Y, Huang J (2011) High-temperature inter-mineral magnesium isotope fractionation in eclogite from the Dabie orogen, China. Earth Planet Sci Lett 304(1):224–230

Li JX, Qin KZ, Li GM, Evans NJ, Zhao JX, Cao MJ, Huang F (2016a) The Nadun Cu-Au mineralization, central Tibet: root of a high sulfidation epithermal deposit. Ore Geol Rev 78:371–387

Li WY, Teng FZ, Xiao Y, Gu HO, Zha XP, Huang J (2016b) Empirical calibration of the clinopyroxene-garnet magnesium isotope geothermometer and implications. Contrib Mineral Petrol 171:61. doi:10.1007/s00410-016-1269-1

Liu DY, Nutman AP, Compston W, Wu JS, Shen QH (1992) Remnants of $\geq$ 3800 Ma crust in the Chinese part of the Sino-Korean craton. Geology 20(4):339–342

Liu CQ, Masuda A, Xie GH (1994) Major- and traceelement compositions of Cenozoic basalts in eastern China: petrogenesis and mantle source. Chem Geol 114:19–42

Liu YS, Yuan HL, Gao S, Hu ZC, Wang X, Liu XM, Lin WL (2004) Zircon U-Pb ages of olivine pyroxenite xenolith from Hannuoba: links between the 97-158 Ma basaltic underplating and granulite-facies metamorphism. Chin Sci Bull 49:1055–1062

Liu YS, Gao S, Lee CTA, Hu SH, Liu XM, Yuan HL (2005) Melt-peridotite interactions: links between garnet pyroxenite and high-Mg# signature of continental crust. Earth Planet Sci Lett 234:39–57

Liu YS, Gao S, Hu ZC, Gao CG, Zong KQ, Wang DB (2010) Continental and oceanic crust recycling-induced melt-peridotite interactions in the Trans-North China Orogen: U-Pb dating, Hf isotopes and trace elements in zircons from mantle xenoliths. J Petrol 51:537–571

Liu SA, Teng FZ, Yang W, Wu FY (2011) High-temperature inter-mineral magnesium isotope fractionation in mantle xenoliths from the North China craton. Earth Planet Sci Lett 308(1):131–140

Macris CA, Manning CE, Young ED (2015) Crystal chemical constraints on inter-mineral Fe isotope fractionation and implications for Fe isotope disequilibrium in San Carlos mantle xenoliths. Geochim Cosmochim Acta 154:168–185

McDonough WF, Frey FA (1989) Rare earth elements in upper mantle rocks. In: Lipin B, McKay G (eds) Geochemistry and mineralogy of rare earth. Elements, Reviews in Minerology, USA

McDonough WF, Sun SS (1995) The composition of the earth. Chem Geol 120:223–253

Melson WG, Vallier TL, Wright TL, Byerly G, Nelen J (1976) Chemical diversity of abyssal volcanic glass erupted along the Pacific, Atlantic and Indian Ocean sea-floor spreading centres. The geophysics of the Pacific Ocean Basin and its margin. American Geophysics Union, Washington, pp 351–368

Menzies MA, Xu YG (1998) Geodynamics of the North China Craton. Mantle dynamics and plate interactions in East Asia, vol 27. AGU, Washington, pp 155–165

Menzies MA, Kempton PD, Dungan M (1985) Interaction of continental lithosphere and asthenospheric melts below the Geronimo Volcanic Field, Arizona, USA. J Petrol 26:663–693

Menzies MA, Fan WM, Zhang M (1993) Palaeozoic and Cenozoic lithoprobes and the loss of >120 km of Archaean lithosphere, Sino-Korean craton, China. Geological Society, London

Menzies MA, Xu YG, Zhang HF, Fan WM (2007) Integration of geology, geophysics and geochemistry: a key to understanding the North China Craton. Lithos 96(1–2):1–21

Morimoto N (1988) Nomenclature of pyroxenes. Can Mineral 27:143–156

Nickel KG, Green DH (1985) Empirical geothermobarometry for garnet peridotites and implications for the nature of the lithosphere, kimberlites and diamonds. Earth Planet Sci Lett 73:158–170

Nimis P, Taylor WR (2000) Single clinopyroxene thermobarometry for garnet peridotites. Part I. Calibration and testing of a Cr-in-Cpx barometer and an enstatite-in-Cpx thermometer. Contrib Mineral Petrol 139:541–554

O'Reilly SY, Griffin WL (2012) Mantle Metasomatism. In: Harlov D, Austrheim H (eds) Metasomatism and the chemical transformation of rock: the role of fluids in terrestrial and extraterrestrial processes (Lecture notes in earth system sciences). Springer-Verlag, Berlin, pp 471–534

Pearson DG, Nowell GM (2004) Re-Os and Lu-Hf isotope constraints on the origin and age of pyroxenites from the Beni Bousera peridotite massif implications for mixed peridotite-pyroxenite mantle sources. J Petrol 45(2):439–455

Pilet S, Baker MB, Stolper EM (2008) Metasomatized lithosphere and the origin of alkaline lavas. Science 320:916–919

Poitrasson F, Halliday AN, Lee DC, Levasseur S, Teutsch N (2004) Iron isotope differences between Earth, Moon, Mars and Vesta as possible records of contrasted accretion mechanisms. Earth Planet Sci Lett 223(3):253–266

Poitrasson F, Delpech G, Grégoire M (2013) On the iron isotope heterogeneity of lithosphericmantle xenoliths: implications for mantlemetasomatism, the origin of basalts and the iron isotope composition of the Earth. Contrib Mineral Petrol 165(6):1243–1258

Qian SP, Ren ZR, Zhang L, Hong LB, Liu JQ (2015) Chemical and Pb isotope composition of olivine-hosted melt inclusions from the Hannuoba basalts, North China Craton:implications for petrogenesis and mantle source. Chem Geol 401:111–125

Richter FM, Watson EB, Mendybaev RA, Teng FZ, Janney PE (2008) Magnesium isotope fractionation in silicate melts by chemical and thermal diffusion. Geochim Cosmochim Acta 72:206220

Richter FM, Watson EB, Mendybaev RA, Dauphas N, Georg RB, Watkins J, Valley JW (2009) Isotopic fractionation of the major elements of molten basalt by chemical and thermal diffusion. Geochim Cosmochim Acta 73:4250–4263

Roskosz M, Sio CK, Dauphas N, Bi WL, Tissot FLH, Hu MY, Zhao JY, Alp EE (2015) Spinel-olivine-pyroxene equilibrium iron isotopic fractionation and applications to natural peridotites. Geochim Cosmochim Acta 169:184–199

Rudnick RL, Gao S, Ling WL, Liu YS, McDonough WF (2004) Petrology and geochemistry of spinel peridotite xenoliths from Hannuoba and Qixia, North China Craton. Lithos 77:609–637

Schauble EA (2004) Applying stable isotope fractionation theory to new systems. Rev Mineral Geochem 55(1):65–111

Schauble EA (2011) First-principles estimates of equilibrium magnesium isotope fractionation in silicate, oxide, carbonate and hexaaquamagnesium(2+) crystals. Geochim Cosmochim Acta 75(3):844–869

Schilling JG, Zajac M, Evans R, Johnston T, White W, Devine JD, Kingsley R (1983) Petrologic and geochemical variations along the Mid-Atlantic Ridge from 27_N to 73_N. Am J Sci 283:510–586

Schoenberg R, Blanckenburg FV (2006) Modes of planetary-scale Fe isotope fractionation. Earth Planet Sci Lett 252(3–4):342–359

Schuessler JA, Schoenberg R, Sigmarsson O (2009) Iron and lithium isotope systematics of the Hekla volcano, Iceland-Evidence for Fe isotope fractionation during magma differentiation. Chem Geol 258(1–2):78–91

Sio CKI, Dauphas N, Teng FZ, Chaussidon M, Helz RT, Roskosz M (2013) Discerning crystal growth from diffusion profiles in zoned olivine by in situ Mg–Fe isotopic analyses. Geochim Cosmochim Acta 123:302–321

Sobolev NV, Lavrent'ev YG, Pokhilenko NP, Usova LV (1973) Chrome-rich garnets from the kimberlites of Yakuti and their parageneses. Contrib Mineral Petrol 40(1):39–52

Sobolev AV, Hofmann AW, Sobolev SV, Nikogosian IK (2005) An olivine-free mantle source of Hawaiian shield basalts. Nature 434:590–597

Song Y, Frey FA (1989) Geochemistry of peridotite xenoliths in basalt from Hannuoba, eastern China: implications for subcontinental mantle heterogeneity. Geochim Cosmochim Acta 53:97–113

Song Y, Frey FA, Zhi XC (1990) Isotopic characteristics of Hannuoba basalts, eastern China: implications for their petrogenesis and the composition of subcontinental mantle. Chem Geol 88(1):35–52

Sossi PA, Foden JD, Halverson GP (2012) Redox-controlled iron isotope fractionation during magmatic differentiation: an example from the Red Hill intrusion, S. Tasmania Contrib Mineral Petrol 164(5):757–772

Strandmann PAP, Elliott T, Marschall HR, Coath C, Lai YJ, Jeffcoate AB, Ionov DA (2011) Variations of Li and Mg isotope ratios in bulk chondrites and mantle xenoliths. Geochim Cosmochim Acta 75(18):5247–5268

Tanaka T, Togashi S, Kamioka H, Amakawa H, Kagami H, Hamamoto T, Yuhara M, Orihashi Y, Yoneda S, Shimizu H, Kunimaru T, Takahashi K, Yanagi T, Nakano T, Fujimaki H, Shinjo R, Asahara Y, Tanimizu M, Dragusanu C (2000) vJNdi-1: a neodymium isotopic reference in consistency with LaJolla neodymium. Chem Geol 168:279–281

Tang YJ, Zhang HF, Nakamura E, Moriguti T, Kobayashi K, Ying JF (2007) Lithium isotopic systematics of peridotite xenoliths from Hannuoba, North China Craton: implications for melt-rock interaction in the considerably thinned lithospheric mantle. Geochim Cosmochim Acta 71:4327–4341

Tatsumoto M, Basu AR, Huang WK, Wang JW, Xie GH (1992) Sr, Nd, and Pb isotopes of ultramafic xenoliths in volcanic-rocks of Eastern China: enriched components EMI and EMII in subcontinental lithosphere. Earth Planet Sci Lett 113:107–128

Teng FZ, Wadhwa M, Helz RT (2007) Investigation of magnesium isotope fractionation during basalt differentiation: implications for a chondritic composition of the terrestrial mantle. Earth Planet Sci Lett 261(1):84–92

Teng FZ, Dauphas N, Helz RT (2008) Iron isotope fractionation during magmatic differentiation in Kilauea Iki Lava Lake. Science 320(5883):1620–1622

Teng FZ, Li WY, Ke S, Marty B, Dauphas N, Huang SC, Wu FY, Pourmand A (2010) Magnesium isotopic composition of the Earth and chondrites. Geochim Cosmochim Acta 74(14):4150–4166

Teng FZ, Dauphas N, Helz RT, Gao S, Huang SC (2011) Diffusion-driven magnesium and iron isotope fractionation in Hawaiian olivine. Earth Planet Sci Lett 308(3–4):317–324

Teng FZ, Dauphas N, Huang SC, Marty B (2013) Iron isotopic systematics of oceanic basalts. Geochim Cosmochim Acta 107:12–26

Teng FZ, Dauphas N, Watkins JM (2017) Non-Traditional Stable Isotopes: retrospective and Prospective. Rev Mineral Geochem 82(1):219–287

Urey HC (1947) The thermodynamic properties of isotopic substance. J Chem Soc 8:562–581

Wang C, Jin ZM, Gao S, Zhang JF, Zheng S (2010) Eclogite-melt/peridotite reaction: experimental constraints on the destruction mechanism of the North China Craton. Sci China Earth Sci 53:797–809

Wang SJ, Teng FZ, Williams HM, Li SG (2012) Magnesium isotopic variations in cratonic eclogites: origins and implications. Earth Planet Sci Lett 359:219–226

Wang SJ, Teng FZ, Li SG (2014a) Tracing carbonate-silicate interaction during subduction using magnesium and oxygen isotopes. Nat Commun 5:5328. doi:10.1038/ncomms6328

Wang SJ, Teng FZ, Li SG, Hong JA (2014b) Magnesium isotopic systematics of mafic rocks during continental subduction. Geochim Cosmochim Acta 143:34–48

Wang SJ, Teng FZ, Bea F (2015a) Magnesium isotopic systematics of metapelite in the deep crust and implications for granite petrogenesis. Geochem Perspect Lett 1:75–83

Wang SJ, Teng FZ, Rudnick RL, Li SG (2015b) Magnesium isotope evidence for a recycled origin of cratonic eclogites. Geology 43:1071–1074

Wells PRA (1977) Pyroxene thermometry in simple and complex systems. Contrib Mineral Petrol 62:129–139

Weyer S, Ionov DA (2007) Partial melting and melt percolation in the mantle: the message from Fe isotopes. Earth Planet Sci Lett 259(1–2):119–133

Weyer S, Seitz HM (2012) Coupled lithium and iron isotope fractionation during magmatic differentiation. Chem Geol 294(2):42–50

Williams HM, Bizimis M (2014) Iron isotope tracing of mantle heterogeneity within the source regions of oceanic basalts. Earth Planet Sci Lett 404:396–407

Williams HM, McCammon CA, Peslier AH, Halliday AN, Teutsch N, Levasseur S, Burg JP (2004) Iron isotope fractionation and the oxygen fugacity of the mantle. Science 304(5677):1656–1659

Williams HM, Peslier AH, McCammon C, Halliday AN, Levasseur S, Teutsch N, Burg JP (2005) Systematic iron isotope variations inmantle rocks and minerals: the effects of partial melting and oxygen fugacity. Earth Planet Sci Lett 235(1–2):435–452

Williams HM, Nielsen SG, Renac C, Griffin WL, O'Reilly SY, McCammon CA, Pearson N, Viljoen F, Alt JC, Halliday AN (2009) Fractionation of oxygen and iron isotopes by partial melting processes: implications for the interpretation of

stable isotope signatures in mafic rocks. Earth Planet Sci Lett 283(1–4):156–166

Williams HM, Wood BJ, Wade J, Frost DJ, Tuff J (2012) Isotopic evidence for internal oxidation of the Earth's mantle during accretion. Earth Planet Sci Lett 321:54–63

Wilshire HG, Shervais JW (1975) Al-augite and Cr-diopside ultramafic xenoliths in basaltic rocks from western United States. Phys Chem Earth 9:257–272

Wu ZQ, Huang F, Huang SC (2015) Isotope fractionation induced by phase transformation: first-principles investigation for Mg_2SiO_4. Earth Planet Sci Lett 409:339–347

Xiao Y, Teng FZ, Zhang HF, Yang W (2013) Large magnesium isotope fractionation in peridotite xenoliths from eastern North China craton: product of melt–rock interaction. Geochim Cosmochim Acta 115:241–261

Xu YG (2001) Thermo-tectonic destruction of the Archean lithospheric keel beneath the Sino-Korean Craton in China: evidence, timing and mechanism. Phys Chem Earth 26:747–757

Xu YG (2002) Evidence for crustal components in the mantle and constrains on crustal recycling mechanism: pyroxenite xenoliths from Hannuoba, North China. Chem Geol 182:301–322

Yang JH, Wu FY, Wilde SA (2003) A review of the geodynamic setting of large-scale Late Mesozoic gold mineralization in the North China Craton: an association with lithospheric thinning. Ore Geol Rev 23(3–4):125–152

Yang W, Teng FZ, Zhang HF (2009) Chondritic magnesium isotopic composition of the terrestrial mantle: a case study of peridotite xenoliths from the North China craton. Earth Planet Sci Lett 288(3):475–482

Ying J, Zhang H, Tang Y, Su B, Zhou X (2013) Diverse crustal components in pyroxenite xenoliths from Junan, Sulu orogenic belt: implications for lithospheric modification invoked by continental subduction. Chem Geol 356:181–192

Young ED, Tonui E, Manning CE, Schauble E, Macris CA (2009) Spinel-olivine magnesium isotope thermometry in the mantle and implications for the Mg isotopic composition of Earth. Earth Planet Sci Lett 288:524–533

Young ED, Manning CE, Schauble EA, Shahar A, Macris CA, Lazar C, Jordan M (2015) High-temperature equilibrium isotope fractionation of non-traditional stable isotopes: experiments, theory, and applications. Chem Geol 395:176–195

Yu SY, Xu YG, Ma JL, Zheng YF, Kuang YS, Hong LB, Ge WC, Tong LX (2010) Remnants of oceanic lower crust in the subcontinental lithospheric mantle: trace element and Sr-Nd-O isotope evidence from aluminous garnet pyroxenite xenoliths from Jiaohe, Northeast China. Earth Planet Sci Lett 297:413–422

Zhang HF, Sun M, Zhou XH, Fan WM, Zhai MG, Ying JF (2002) Mesozoic lithosphere destruction beneath the North China Craton: evidence from major-, trace-element and Sr-Nd-Pb isotope studies of Fangcheng basalts. Contrib Mineral Petrol 144:241–253

Zhang HF, Sun M, Zhou XH, Ying JF (2005) Geochemical constraints on the origin of Mesozoic alkaline intrusive complexes from the North China Craton and tectonic implications. Lithos 81(1):297–317

Zhang HF, Goldstein SL, Zhou XH, Sun M, Cai Y (2009a) Comprehensive refertilization of lithospheric mantle beneath the North China Craton: further Os-Sr-Nd isotopic constraints. J Geol Soc 166(2):249–259

Zhang JJ, Zheng YF, Zhao ZF (2009b) Geochemical evidence for interaction between oceanic crust and lithospheric mantle in the origin of Cenozoic continental basalts in east-central China. Lithos 110:305–326

Zhang HF, Nakamura E, Kobayashi K, Ying JF, Tang YJ (2010) Recycled crustal melt injection into lithospheric mantle: implication from cumulative composite and pyroxenite xenoliths. Int J Earth Sci 99(6):1167–1186

Zhang JF, Wang C, Wang YF (2012) Experimental constraints on the destruction mechanism of the North China Craton. Lithos 149:91–99

Zhao GC, Sun M, Wilde SA, Li SZ (2005) Late Archean to Paleoproterozoic evolution of the North China Craton: key issues revisited. Precambrian Res 136(2):177–202

Zhao XM, Zhang HF, Zhu XK, Tang SH, Tang YJ (2010) Iron isotope variations in spinel peridotite xenoliths fromNorth China Craton: implications for mantlemetasomatism. Contrib Mineral Petrol 160(1):1–14

Zhao XM, Zhang HF, Zhu XK, Tang SH, Yan B (2012) Iron isotope evidence for multistage melt-peridotite interactions in the lithospheric mantle of eastern China. Chem Geol 292–293:127–139

Zhao XM, Zhang HF, Zhu XK, Zhu B, Cao HH (2015) Effects of melt percolation on iron isotopic variation in peridotites from Yangyuan, North China Craton. Chem Geol 401:96–110

Zhao XM, Zhang ZF, Huang SC, Liu YF, Li X, Zhang ZF (2017) Coupled extremely light Ca and Fe isotopes in peridotites. Geochim Cosmochim Acta. doi:10.1016/j.gca.2017.03.024

Zheng JP, O'reilly SY, Griffin WL, Lu FX, Zhang M (1998) Nature and evolution of Cenozoic lithospheric mantle beneath Shandong peninsula, Sino-Korean Craton, eastern China. Int Geol Rev 40(6):471–499

Zheng JP, Griffin WL, O'Reilly SY, Yang JS, Li TF, Zhang M, Zhang RY, Liou JG (2006) Mineral chemistry of peridotites from Paleozoic, Mesozoic and Cenozoic lithosphere: constraints on mantle evolution beneath eastern China. J Petrol 47(11):2233–2256

Zheng JP, Griffin WL, O'Reilly SY, Yu CM, Zhang HF, Pearson N, Zhang M (2007) Mechanism and timing of lithospheric modification and replacement beneath theeastern North China Craton: peridotitic xenoliths from the 100 Ma Fuxin basalts anda regional synthesis. Geochim Cosmochim Acta 71(21):5203–5225

Zheng JP, Griffin WL, Qi L, O'Reilly SY, Sun M, Zheng S, Pearson N, Gao JF, Yu CM, Su YP, Tang HY, Liu QS, Wu XL (2009) Age and composition of granulite and pyroxenite xenoliths in Hannuoba basalts reflect Paleogene underplating beneath the North China Craton. Chem Geol 264:266–280

Zhi XC, Song Y, Frey FA, Feng JL, Zhai MG (1990) Geochemistry of Hannuoba basalts, eastern China: constraints on the origin of continental alkalic and tholeiitic basalt. Chem Geol 88:1–33

Zhu BQ (1998) Theory and Applications of Isotope Systematics in Geosciences: Evolution of Continental Crust and Mantle in China (in Chinese). Science Press, Beijing

Zhu XK, Guo Y, Williams RJP, O'Nions RK, Matthews A, Belshaw NS, Canters GW, Waal EC, Weser U, Burgess BK, Salvato B (2002) Mass fractionation processes of transition metal isotopics. Earth Planet Sci Lett 200(1–2):47–62